Bulletin of the Geological Society of Finland, Vol. 96, 2024, pp 135–160 https://doi.org/10.17741/bgsf/96.2.002

Paleoproterozoic post-orogenic magmatism in southern Finland; geochemical, geochronological and Sr-Nd isotopic constraints on origin and magmatic evolution

Oliver Teräs[1,*], Kaisa Nikkilä[1], Perttu Mikkola[2], Anna Kotilainen[3], Olav Eklund[1] and O. Tapani Rämö[3]

[1] *Åbo Akademi University, Department of Geology and Mineralogy, Akatemiankatu 1, 20500 Turku, Finland*

[2] *Geological Survey of Finland, Viestikatu 7A, 70211 Kuopio, Finland*

[3] *University of Helsinki, Department of Geosciences and Geography, Geology and Geophysics Research Program, Gustaf Hällströmin katu 2, 00014 Helsinki, Finland*

Abstract

Fifteen post-orogenic, basic to acidic High-Barium-Strontium (HiBaSr) intrusions of shoshonitic affinity have been recognized in central and southern Finland. Most of the intrusions are found in a 500 km long E–W-trending belt in the Southern Finland Subprovince, with three of them in the Western Finland Subprovince. These rocks have distinctive field, mineralogical, chemical, geochronological and isotopic characteristics compared to the other plutonic rocks in the area. New zircon U-Pb LA-ICP-MS data for two of the intrusions confirm their post-orogenic age: 1805 ± 4 Ma for the Tistronskär biotite-hornblende monzodiorite and 1794 ± 13 Ma for the fluorite-bearing Loukee biotite granite. These rocks plot predominantly in the shoshonitic field and have relatively high K_2O (~2.3 wt.%) in the basic varieties, increasing to ~5.0 wt.% in more acidic types. The Tistronskär monzodiorite and Loukee granite show similar geochemistry (high K, Ti, P, Ba, Sr and LREE) to other shoshonitic rocks in southern Finland. These geochemical characteristics, along with an initial $^{87}Sr/^{86}Sr$ value of 0.70322 and initial εNd value of -0.4 ± 0.4 at 1805 Ma for Tistronskär monzodiorite, indicate that subcontinental lithospheric mantle source may have been metasomatized by subducted sedimentary material before the 1.80 Ga melting event.

Keywords: Svecofennian, Paleoproterozoic, post-orogenic magmatism, High Ba-Sr granites, U-Pb, Sm-Nd, Rb-Sr, Tistronskär, Loukee

* Corresponding author. E-mail address: oliver.teras@abo.fi

Editorial handling: Jarmo Kohonen (email: jarmo.kohonen@helsinki.fi)

1. Introduction

Post-orogenic magmatism occurs in an orogenic cycle after the major horizontal terrane movements have ceased. This transition from orogenic to post-orogenic phase thus marks also the end of the orogenic period (Liégeois 1998). During the shift to the post-orogenic phase, the magmatism typically changes gradually to more shoshonitic (Bonin et al. 1998; Liégeois et al. 1998). Acidic rocks belonging to the shoshonite series are usually classified as High-Barium-Strontium (HiBaSr) granitoids (Tarney & Jones 1994), which is a group distinct from, but complementary to the more traditional classification into I-, S- and A-type granites (Whalen et al. 1987; Chappell & White 2001). The HiBaSr rocks are characterized by high K_2O, TiO_2, P_2O_5, Ba, Sr and LREE content relative to the calc-alkaline rocks. In multi-element plots, HiBaSr rocks (basic to acidic) show subduction-related negative Nb and Ta anomalies and lack of pronounced Eu anomalies (Fowler et al. 2008; Ye et al. 2008; Nardi et al. 2021). All these geochemical characteristics indicate that their source areas had been modified by subducted material and were plagioclase free or highly oxidized (Fowler et al. 2008; Couzinié et al. 2016). The HiBaSr acidic rocks associated with parental basic (lamprophyric/appinitic) magmas are well-known from the British Caledonian Province (Fowler et al. 2008), the Tibetan Plateau (Ye et al. 2008), the Dom Feliciano Belt of Southern Brazil (Nardi et al. 2021), Antarctica (Rocchi et al. 2009), as well as southern Finland (Eklund et al. 1998; Rutanen et al. 2011).

In southern Finland, these intrusions have been called post-orogenic (Simonen 1980), post-collisional (Eklund et al. 1998) or post-kinematic (Rutanen et al. 2011). In this study, we use the term post-orogenic as defined by Bonin et al. (1998) and Liégeois (1998). We use the post-orogenic term for shoshonitic HiBaSr rocks found in the Svecofennian province, and they are considered post-orogenic in relation to the Svecofennian orogeny.

Multiple origins have been proposed for the HiBaSr acidic magmatism. One model suggests that the acidic melts are results of continuous fractional crystallization starting from trachy-basaltic parent (e.g., Duchesne et al. 1998; Eklund et al. 1998; Mohamed 1998; Qian et al. 2003; Meng et al. 2018). Another model suggests that the trachy-basaltic and acidic rocks crystallized from two genetically independent melts, with the trachy-basalts originating from the mantle and the acidic melts from the melting of the lower crust (Bitencourt & Nardi 2004; Choi et al. 2008; Ye et al. 2008; Lara et al. 2017; Martini et al. 2019). Also, mixing of mantle-derived magmas with crustal melts has been proposed as a model for the genesis of HiBaSr granites (Thompson & Fowler 1986; Lindberg & Eklund 1988; Zhang et al. 2015), as well as derivation directly by partial melting of a metasomatized mantle source (Jiang et al. 2012; Gómez-Frutos et al. 2023). Obviously, several fundamental questions remain open and need to be addressed to answer how HiBaSr systems are related to mantle/crustal melting, granite petrogenesis, and the formation of bimodal plutons (Keller et al. 2015; Clemens et al. 2022).

Experimental studies show that trachy-basaltic magmas are mostly formed by melting of metasomatized upper mantle wehrlite or pyroxenite (Wyllie & Sekine 1982; Condamine & Médard 2014; Förster et al. 2019; Becerra-Torres et al. 2020). Trachy-basaltic magmas are relatively scarce along the continental arcs compared to basalts or basaltic andesites. Therefore, trachy-basaltic melts and their equivalent plutonic rocks (monzogabbros) offer valuable insight into the composition of the upper mantle and the geodynamic conditions during the late stage of an ancient orogeny such as the Svecofennian orogeny in southern Finland.

This study reports the mineralogy, whole-rock geochemical composition, zircon U-Pb geochronology and whole-rock Sr-Nd isotopes of the Tistronskär monzodiorite and the Loukee granite, the new discoveries of basic and acidic members of the post-orogenic magmatic suite of southern and western Finland. To evaluate the origin of the intrusions, their geochemical characteristics are compared with the other post-orogenic magmatic rocks in southern Finland.

2. Geological background

2.1. Svecofennian orogen

The Svecofennian multi-phase accretionary orogeny took place at 1.92−1.76 Ga and caused the growth and thickening of the Paleoproterozoic crust in Finland and adjacent areas (Fig. 1; Nironen 1997, 2017; Lahtinen et al. 2005, 2023; Korja et al. 2006). Collision between the blocks forming central and southern Finland occurred at 1.89−1.88 Ga (Lahtinen et al. 2005) and even present day, the upper lithosphere of central and southern Finland is characterized by an anomalously thick crust (up to 65 km) with a high-velocity lower crust (Korja et al. 1993; Janik et al. 2007; Lahtinen et al. 2009). The high-velocity lower crust is interpreted to represent eclogitized lower crust and/or mafic garnet granulites overlaying peridotitic upper mantle (Janik et al. 2007) or to consist of a mixture of hornblendites, mafic garnet granulites, pyroxenites and mafic eclogites (Kuusisto et al. 2006). Hereafter, the bedrock domains in central and southern Finland are referred to as the Western Finland Subprovince (WFS) and Southern Finland Subprovince (SFS), respectively (Nironen 2017; Figs. 1 and 2).

In the WFS, the oldest primitive arc magmatism at 1.93–1.91 Ga (Vaasjoki et al. 2003; Huhma et al. 2021) and syn-orogenic bimodal magmatism at 1.90–1.87 Ga (Nironen et al. 2000; Peltonen 2005; Makkonen 2015; Nikkilä et al. 2016) were the main magmatic events. The volcanic rocks are associated with sedimentary, mainly turbiditic sequences; now paraschists, paragneisses and metagreywackes (Lahtinen 2000; Lahtinen et al. 2002). Together, these assemblages form a curvilinear belt that extends from Tampere to the Ostrobothnian Schist Belt, encircles the Vaasa Complex and continues to north-central Sweden (Fig. 2; Nironen 2017; Chopin et al. 2020; Lahtinen et al. 2023). Granitic pegmatites (~1.80−1.79 Ga; Alviola et al. 2001) represent the youngest magmatic activity in the WFS.

In the SFS, the bedrock is dominated by 1.91–1.85 Ga metasedimentary and 1.90–1.88 Ga syn-orogenic ultrabasic-acidic volcanic/plutonic rocks with arc-type geochemical characteristics (Lahtinen 1996; Väisänen and Mänttäri 2002; Kähkönen 2005; Bergman et al. 2008; Kara et al. 2018; Lahtinen et al. 2022), intra-orogenic basic volcanic/plutonic rocks at 1.86−1.85 Ga (Pajunen et al. 2008; Väisänen et al. 2012; Nevalainen et al. 2014; Kara et al. 2020), late-orogenic leucogranites at 1.84−1.82 Ga (Ehlers et al. 1993; Kurhila et al. 2005, 2011; Andersen & Rämö 2021), post-orogenic shoshonitic intrusions at 1.81−1.76 Ga (Eklund et al. 1998; Väisänen et al. 2000; Andersson et al. 2006; Rutanen et al. 2011) and anorogenic rapakivi granites at 1.64−1.58 Ga (Rämö & Haapala 2005; Heinonen et al. 2017).

The post-orogenic intrusions (1.81−1.76 Ga) are found throughout the Fennoscandian Shield (Fig. 1). The intrusions lack deformational features (Branigan 1987; Hubbard & Branigan 1987; Rutanen et al. 2011) and are interpreted to have emplaced during a period of uplift or extensional settings that followed the orogeny (Väisänen et al. 2000). The post-orogenic rocks can vary in their geochemistry, with the most common type being shoshonitic, ranging from basic apatite-rich potassic lamprophyres to peraluminous HiBaSr granites (Eklund et al. 1998). There are several suggestions for the melting mechanism of the source of the shoshonitic intrusions including, upwelling of hot asthenospheric material caused by plume activity (Peltonen et al. 2000), convective thinning of the lithosphere (Väisänen et al. 2000), slab break-off event (Eklund & Shebanov 2002; Saalmann et al. 2009), delamination (Kosunen 2004), gravitational collapse enhanced by lithospheric delamination (Korja et al. 2006) or the decay of radioactive isotopes (Kukkonen & Lauri 2009). Also, the Transscandinavian Igneous Belt (TIB) in south-central Sweden (Fig. 1; Högdahl et

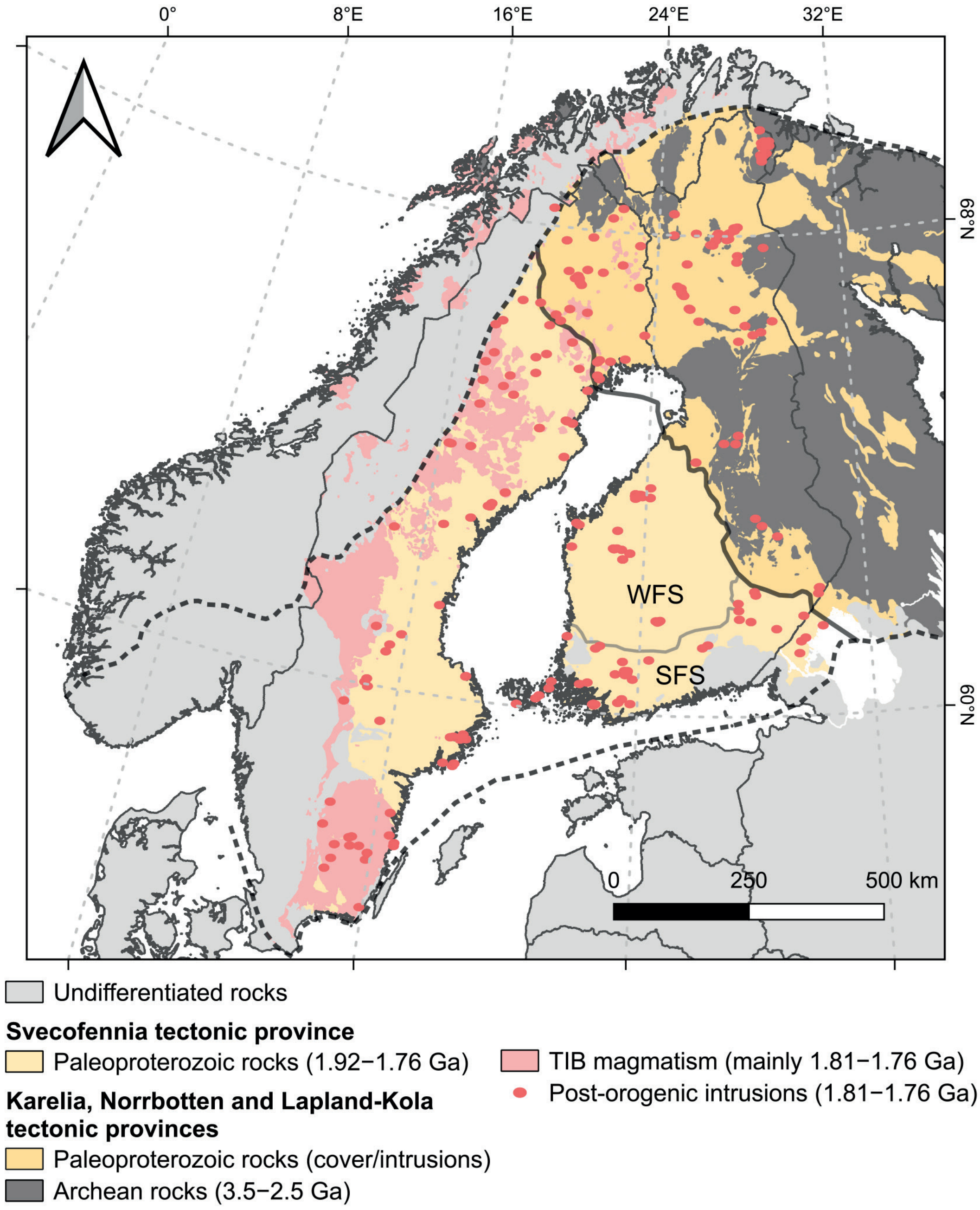

Fig. 1. Post-orogenic magmatism in the Fennoscandian shield during 1.81−1.76 Ga. WFS = Western Finland Subprovince, SFS = Southern Finland Subprovince and TIB = Transscandinavian Igneous Belt. Map modified after Geological map of Finland – Bedrock 1:1 000 000 © Geological Survey of Finland 2016, Geological map of Sweden – Bedrock 1:1 000 000 © Geological Survey of Sweden 2022 and Geological map of Norway – Bedrock 1:1 350 000 © Geological Survey of Norway 2024. References to the post-orogenic intrusions: Eklund et al. 1998; Andersson et al. 2006; Ahtonen et al. 2007; Rutanen et al. 2011; Lauri et al. 2012; Geological Survey of Finland 2014; Heilimo et al. 2014; Woodard and Huhma 2015; Rasilainen et al. 2018, 2023; Geological Survey of Sweden 2022. Svecofennia - Karelia/Norrbotten province boundary shown by black line and subprovince boundary between the WFS and SFS shown by grey line (after Nironen 2017). The boundary of the Fennoscandian shield is shown as dotted line.

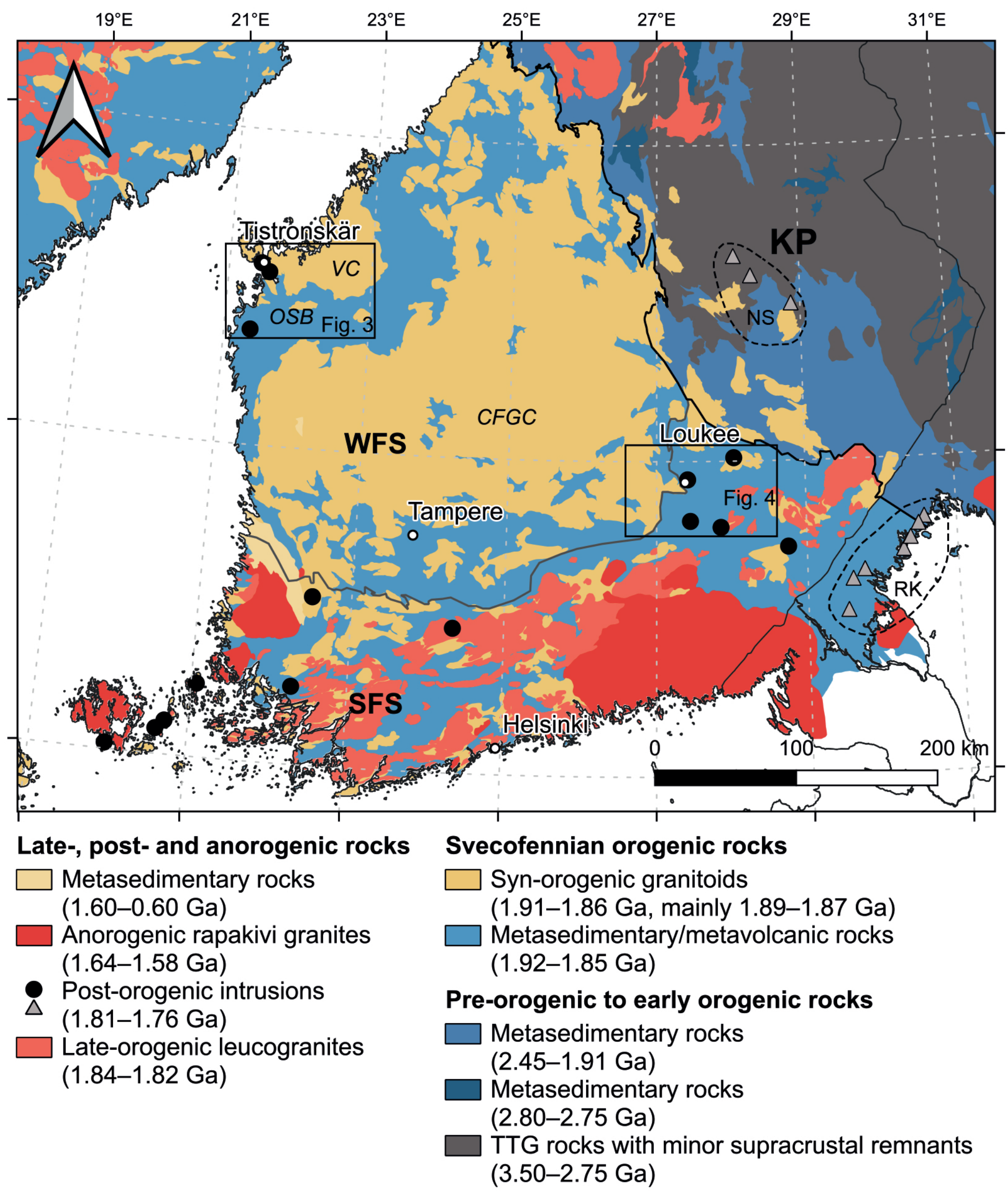

Fig. 2. Lithological map of southern Finland. Boxes indicate locations of Figures 3 and 4. Map modified after Geological map of Finland – Bedrock of Finland 1:5 000 000 © Geological Survey of Finland 2019. KP = Karelia province, WFS = Western Finland Subprovince, SFS = Southern Finland Subprovince, VC = Vaasa Complex, OSB = Ostrobothnian Schist Belt, CFGC = Central Finland Granitoid Complex, NS = North Savo and RK = Russian Karelia. Province boundary shown by black line and subprovince boundary between the WFS and SFS shown by grey line (after Nironen 2017).

al. 2004; Wahlgren & Stephens 2020; Sundblad et al. 2021), a partially simultaneous event (1.81−1.76 Ga) with the emplacement of the post-orogenic magmatic rocks, has been suggested to be related to the post-orogenic intrusions (Andersson et al. 2006). The TIB formed in active continental margin and back-arc extension environments (Högdahl et al. 2004; Wahlgren & Stephens 2020; Sundblad et al. 2021), indicating active subduction at the edge of present-day Fennoscandia (Proto-Baltica) during supercontinent build up (Nironen 2017; Johnsson et al. 2022; Hinchey et al. 2023).

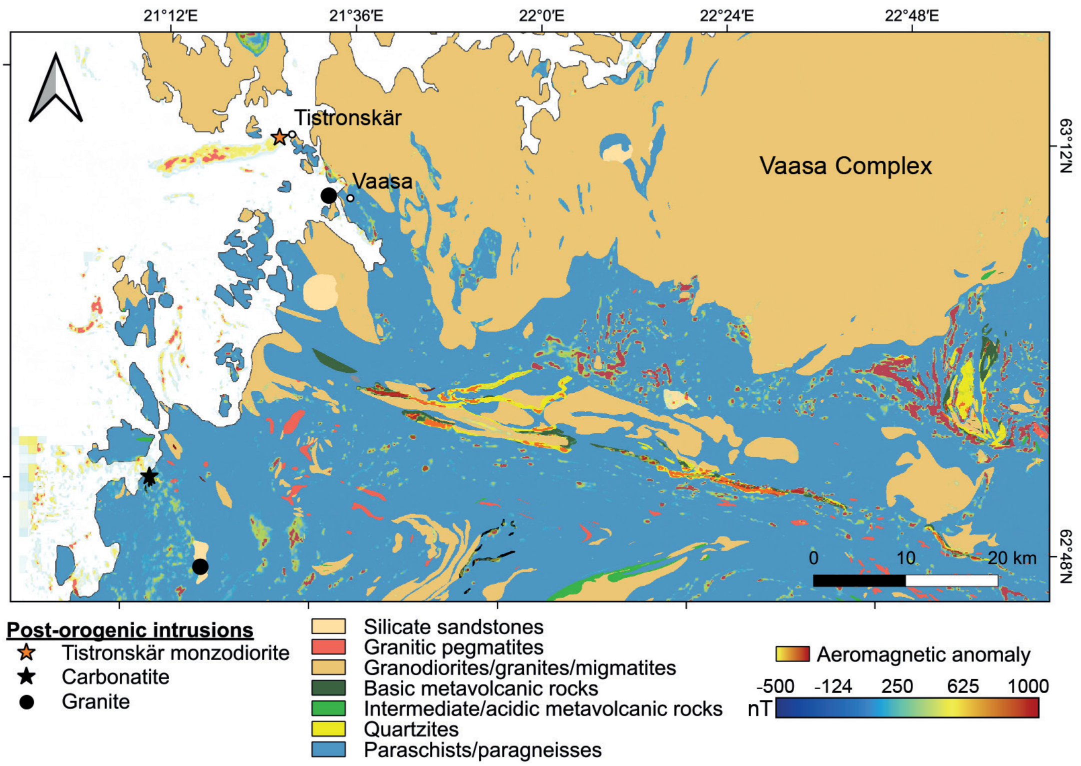

Fig. 3. Geological-magnetic map of the Vaasa area. The Tistronskär monzodiorite shows a strong magnetic anomaly in the aeromagnetic anomaly distribution combined with the lithologic units of the area. nT = nanoTesla, indicating the value of total magnetic field. Map modified after Geological map of Finland – Bedrock 1:200 000 © Geological Survey of Finland 2022 and Aeromagnetic anomaly map of Finland © Geological Survey of Finland 2016.

2.2. Study areas

The research was conducted in two different study areas (Fig. 2), Tistronskär and Loukee. The former represents the WFS, and the latter represents the SFS.

2.2.1. Tistronskär area

Tistronskär is located in the WFS in the vicinity of the Vaasa Complex (Fig. 2). The oldest rock units in the area are turbiditic paragneisses with a maximum deposition age of 1.92–1.91 Ga (Fig. 3; Lahtinen et al. 2017 and reference therein). Basalts, basaltic andesites and graphite-bearing schists are present as interbeds within the turbidites. According to Mäkitie et al. (2012) and Chopin et al. (2020), the granitic rocks represent in situ melting of the adjacent sedimentary rocks, which is also supported by the observed εNd values (Suikkanen et al. 2014). The Tistronskär monzodiorite has been interpreted as part of the syn-orogenic magmatic plutonic rocks of the VC (Sipilä et al. 2017).

The Tistronskär monzodiorite is exposed on a few small islands and skerries close to Vaasa (Lehtonen et al. 2003). On the aeromagnetic map, the intrusion causes an east-west trending 14 km long and 2 km wide anomaly (Fig. 3). Another example of post-orogenic magmatism in the area is the Korsnäs Pb-REE deposit (Fig. 3), which is located about 25 km south of Tistronskär. The 1.825 Ga deposit comprises a network of several hundred carbonate dikes and veins, ranging in width from centimeters to meters, and one larger mass, the Svartören dike (Papunen 1986; Torppa & Karhu 2013).

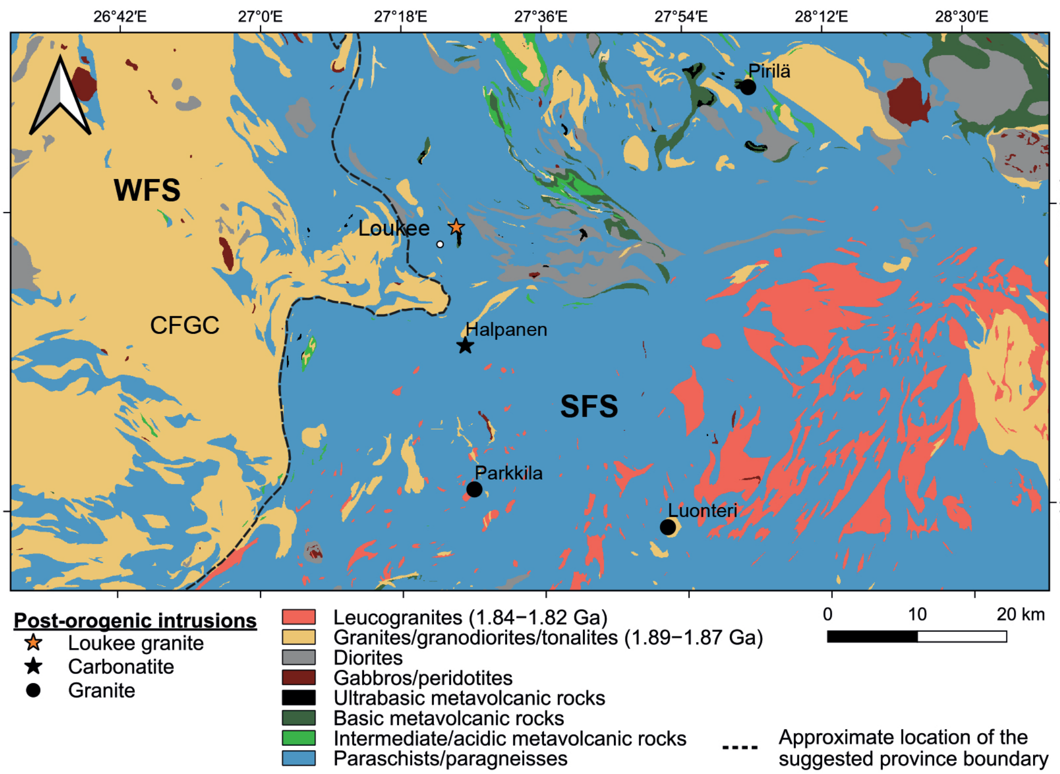

Fig. 4. Geological map of the Loukee area. WFS = Western Finland Subprovince, SFS = Southern Finland Subprovince and CFGC = Central Finland Granitoid Complex. Map modified after Geological map of Finland – Bedrock 1:200 000 © Geological Survey of Finland 2022.

2.2.2. Loukee area

Loukee is located in the SFS, on the southeastern fringe of the Central Finland Granitoid Complex (Fig. 2), in an area dominated by metasedimentary rocks (Fig. 4). Based on the detrital zircon population, the maximum deposition age of the paragneisses in the area is ~1.90 Ga (Mikkola et al. 2018). Their protoliths were deposited in a passive margin setting and subsequently metamorphosed during the main collisional phase of the Svecofennian orogeny into garnet-, cordierite-, and sillimanite-bearing schists and gneisses (Kähkönen 2005). Ultrabasic to basic volcanic rocks, quartz-feldspar gneisses and carbonate rocks are found as interbeds (Pekkarinen 2002). Strong magnetic anomalies have been interpreted as black shales (Hyvönen et al. 2013; Loukola-Ruskeeniemi et al. 2023). The supracrustal sequence was intruded by 1.89–1.87 Ga granitoids and 1.84−1.82 Ga leucogranites (Nironen et al. 2000; Pekkarinen 2002; Kurhila et al. 2011; Heilimo et al. 2018). At 1.80 Ga, post-orogenic granitic intrusions (Parkkila, Luonteri and Pirilä; Rutanen et al. 2011) and a carbonatite dyke (Halpanen; Rukhlov & Bell 2010) were emplaced (Fig. 4). The Loukee granite dykes have not been previously described. They crosscut a small segment (3.0 x 0.5 km) consisting of ultrabasic and basic volcanic rocks interpreted as being erupted at 1.91–1.90 Ga (Kousa et al. 2018). Five U-Th-rich zircons from an amphibolite dyke cutting ultrabasic volcanic rocks were interpreted to indicate a metamorphic event at ~1.8 Ga (Kousa et al. 2018).

3. Methods

3.1. *Major and trace element geochemistry*

One sample from Tistronskär monzodiorite was analyzed at Acme Analytical Laboratory in Vancouver, Canada. The sample was pulverized in a mild steel swing mill. After the $LiBO_2$ fusion and HNO_3 dilution, the major elements and Cr were analyzed by ICP-ES (inductively coupled plasma emission spectrometry). The other trace elements were analyzed by ICP-MS (inductively coupled plasma mass spectrometry).

A total of 8 granitic samples from a drill core (N5112015R9, Loukee granite) were collected for major and trace element analyses. Samples were prepared at the CRS Minlab Oy facility in Kempele, Finland, and samples were analyzed at the MSALABS laboratory in Terrace, Canada. Samples were dried, crushed, and pulverized with an LM5 mill to 70% passing 2 mm, then a representative split was taken and pulverized to 85% passing 75 µm. After the $LiBO_2$ fusion and HNO_3 dilution, major-elements were analyzed by ICP-ES. Refractories and REEs (rare earth elements) were analyzed by ICP-MS. Au, Bi, Hg, Sb, Se and Tl elements were analyzed by ICP-MS, combined with $LiBO_2$ fusion and the true aqua regia solution technique. Ag, Cd, Co, Cu, Mo, Ni, Pd and Zn elements were measured using the ICP-MS system, combined with $LiBO_2$ fusion and the 4-acid solution technique. The F element was measured using an ISE system (ion selective electrode), combined with a fluoride specific fusion technique. Whole-rock geochemical data can be found in Electronic Appendix A.

3.2. *Zircon U-Pb geochronology*

Zircon U-Pb dating was performed at the laboratory of the Geological Survey of Finland in Espoo (Tistronskär monzodiorite and Loukee granite). Zircon grains were selected by handpicking after heavy liquid and magnetic separation. The grains were mounted in epoxy resin, sectioned approximately in half, and polished. BSE images (back-scattered electron) were taken to target the spot analysis sites. For Tistronskär monzodiorite, the analyses were performed using a Nu Plasma HR multicollector ICP-MS and for Loukee granite using a Nu Plasma AttoM single collector ICP-MS. More detailed sample preparation procedures are available in Kotilainen et al. (2016) and in Molnár et al. (2018). The age calculations and plotting of the U-Pb data were done using the IsoplotR program version 6.2 (Vermeesch 2018). All the ages were calculated and plotted with 2σ errors and without decay constant errors. The zircon U-Pb data and BSE images can be found in Electronic Appendix B.

3.3. *Sm-Nd and Sr-Rb isotope geochemistry*

A whole-rock powder was made from the Tistronskär monzodiorite (sample GBTIST) using a swing mill, and ~200 mg of the powder was dissolved in a Savillex teflon screw-cap beaker on a hot plate for 48 hours. After evaporation, the samples were dissolved in HCl to obtain a clear solution. The clear HCl solution was totally spiked with ^{149}Sm-^{150}Nd and ^{87}Rb-^{84}Sr tracers. Rb, Sr, and LREEs were separated using standard cation exchange chromatography, and Sm and Nd were purified using a modified version of the Teflon-HDEHP method of Richard et al. (1976). The total procedural blanks were < 2 ng for Sr and < 300 ng for Nd. Isotopic ratios of Sr, Sm, and Nd were measured on a VG SECTOR 54 mass spectrometer (those of Nd and Sr in dynamic mode). Isotope dilution for Rb was performed on a non-commercial Nier-type mass spectrometer built at the Geological Survey of Finland. Nd isotopic ratios were normalized to $^{146}Nd/^{144}Nd = 0.7219$. Repeated analyses of the La Jolla Nd standard (Lugmair & Carlson 1978) during the time when GBTIST was measured gave $^{143}Nd/^{144}Nd$ of 0.511852 ± 0.000013 (mean and external 2σ error of 63 measurements). The external 2σ error on $^{143}Nd/^{144}Nd$ is 0.0025 % and the Sm-Nd ratios

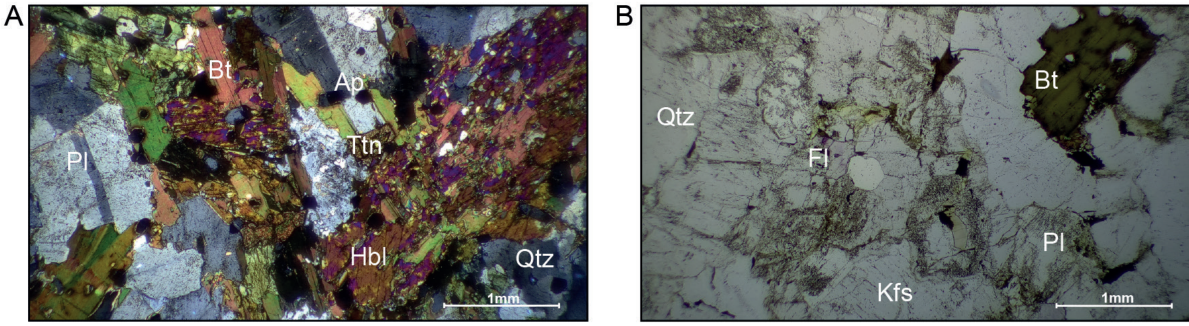

Tistronskär monzodiorite

Loukee granite

Fig. 5. Photomicrographs of the studied rocks. a) Tistronskär monzodiorite in cross-polarized light. b) Loukee granite in plane-polarized light. Qtz = quartz, Pl = plagioclase, Kfs = potassium feldspar, Bt = biotite, Hbl = hornblende, Fl = fluorite, Ap = apatite and Ttn = titanite.

are estimated to be accurate within 0.5 %. The maximum error in the εNd values is ± 0.4 ε-units. Sr isotopic ratios were normalized to $^{86}Sr/^{88}Sr = 0.1194$ (Steiger & Jäger 1977). Repeated analyses of the NBS 987 Sr standard (Moore et al. 1982) yielded $^{87}Sr/^{86}Sr$ of 0.710268 ± 0.000042 (mean and external 2σ error of 23 measurements). The $^{87}Sr/^{86}Sr$ are reported relative to $^{87}Sr/^{86}Sr = 0.71024$. The external 2σ error on $^{87}Sr/^{86}Sr$ is better than 0.006 % and Rb-Sr ratios are estimated to be accurate within 0.5 %. The initial εNd value was calculated using $\lambda^{147}Sm = 6.524 \times 10^{-12}\,a^{-1}$, $^{147}Sm/^{144}Nd = 0.1966$ and $^{143}Nd/^{144}Nd = 0.512638$ (Jacobsen & Wasserburg 1984). The depleted mantle model age was calculated after DePaolo (1981). The initial $^{87}Sr/^{86}Sr$ value was calculated using $\lambda^{87}Rb = 1.3972 \times 10^{-11}\,a^{-1}$ (Villa et al. 2015).

4. Results

4.1. Petrography

The Tistronskär monzodiorite is an even-grained plagioclase (~35 %), biotite (~33 %) and hornblende (~20 %) rich rock with interstitial quartz (~9 %) and accessory titanite, apatite, calcite, and opaque minerals (Fig. 5a). It seems that hornblende and biotite crystallized first, together with apatite. Later, a younger generation of biotite grew at the cost of amphibole. Simultaneously, with the growth of the younger biotite, titanite formed. The plagioclase is altered to sericite and in some places to calcite. Euhedral apatite is common in interstitial quartz. Eklund & Fröjdö (2012) considered that apatite and quartz had grown together in a late phase of crystallization. The rock shows weak signs of deformation with kink bands in biotite and undulating quartz.

The even-grained Loukee biotite granite contains accessory fluorite, muscovite, calcite, titanite, apatite and zircon (Fig. 5b). The grain size of the widest fluorite-bearing dyke change from medium-grained (1–5 mm) to coarse-grained (5–50 mm) to pegmatitic (100–200 mm), and the color from grey to pink, respectively. Fluorite is usually found as an accessory mineral in the groundmass (Fig. 5b) and in coarser-grained variants in miarolitic cavities consisting of fluorite and calcite. Apatite and zircon are present as small crystals.

4.2. Major and trace element geochemistry

The Tistronskär monzodiorite plots in the field between monzodiorite and gabbroic diorite in the TAS diagram (Fig. 6a) and shows a marginal shoshonitic affinity in the Si_2O versus K_2O diagram

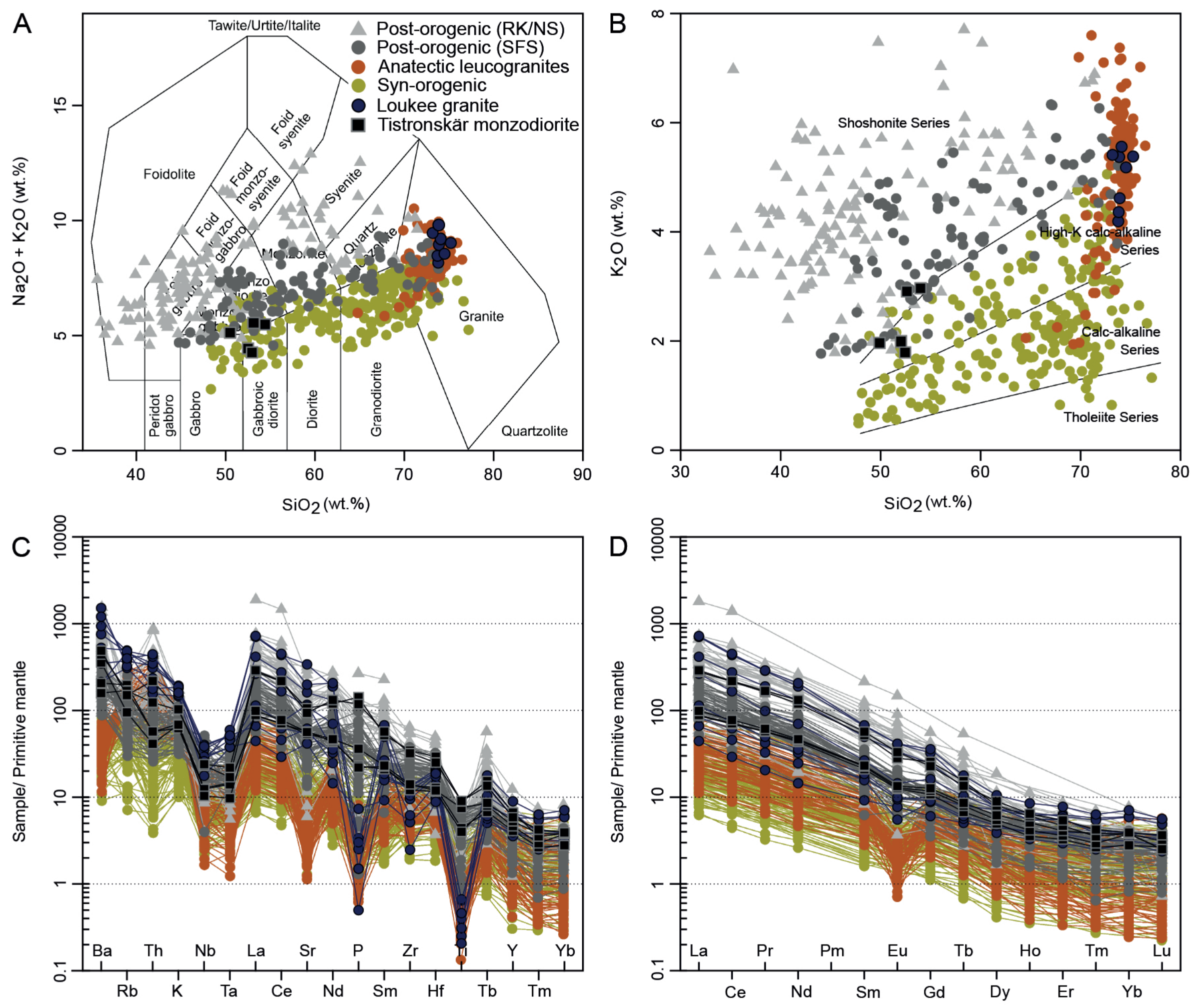

Fig. 6. Tistronskär monzodiorite and Loukee granite compared to other plutonic rocks from the Southern Finland Subprovince (SFS), North Savo (NS) and Russian Karelia (RK). a) SiO_2 versus $Na_2O + K_2O$ diagram after Middlemost (1994). b) SiO_2 versus K_2O diagram after Peccerillo and Taylor (1976). c) Multi-element plot normalized to primitive mantle after McDonough & Sun (1995). d) REE diagram normalized to primitive mantle after McDonough & Sun (1995). References to the post-orogenic rocks can be found in Electronic Appendix A and data to the other plutonic rocks in database of Rock geochemical data of Finland (Geological Survey of Finland 2014).

(Fig. 6b). Total alkalis ($K_2O + Na_2O$) range from 4.2 to 5.5 wt.%. Cr and Ni contents range from 290 to 528 ppm and 76 to 100 ppm, respectively. Ba and Sr contents range from 1045 to 3219 ppm and 1069 to 2107 ppm, respectively. In the primitive mantle-normalized multi-element plot (Fig. 6c), the monzodiorite has a pattern similar to that of basic/intermediate post-orogenic rocks from the SFS (Eklund et al. 1998), showing clear negative anomalies for Nb and Ta and smaller ones for Sr and Ti. In primitive mantle-normalized REE diagram (Fig. 6d), the monzodiorite is strongly enriched in LREEs with La_N of ~169 and $(La/Yb)_N$ of ~46. Monzodiorite also lacks an Eu anomaly (average Eu/Eu* = 0.82; Fig. 6d).

The Loukee granite plots within the granite field in the TAS diagram (Fig. 6a). It is characterized by high SiO_2 (70.2–74.8 wt.%) and K_2O (4.2–5.4 wt.%) with a K_2O/Na_2O ratio of 1.0–1.6, displaying high-K calc-alkaline to weakly

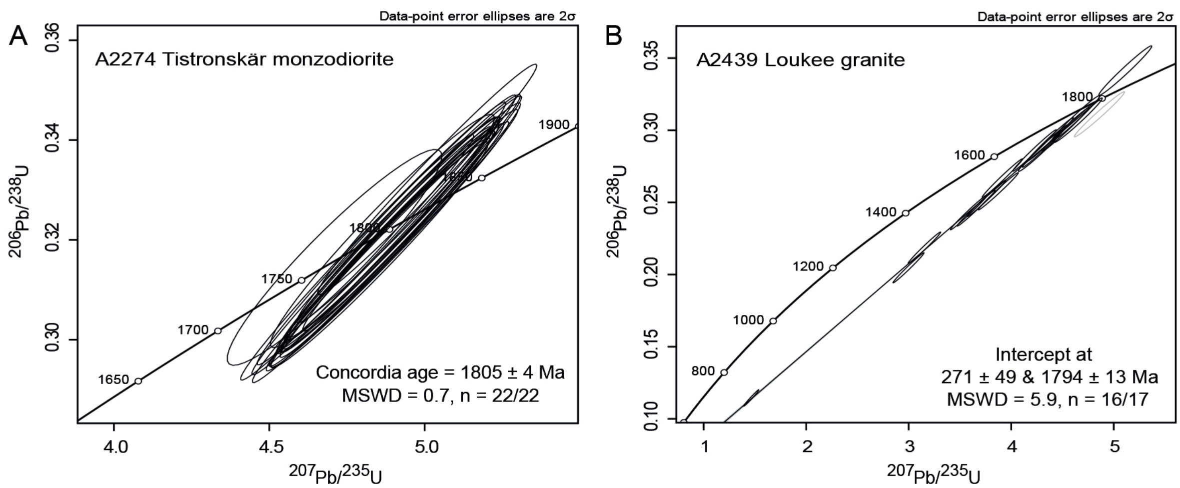

Fig. 7. Concordia plots for the studied samples. n = number of analyses used for the calculation from the total analyzed. MSWD = the Mean Square of the Weighted Deviates for concordance + equivalence/the linear fit. U-Pb data can be found in Electronic Appendix B. a) Sample A2274 (Tistronskär monzodiorite). b) Sample A2439 (Loukee granite). The pale ellipse is excluded from the calculation as inherited.

shoshonitic affinities (Fig. 6b). The granites show large negative anomalies for Nb, Ta, P, Ti and smaller one for Zr (Fig. 6c), and they are enriched in LREEs with La_N up to ~722 and $(La/Yb)_N$ up to 188 (Fig. 6d). Granites are strongly enriched in LILEs such as Ba (1359 to >10000 ppm) and Sr (827−6752 ppm) and lack significant Eu anomalies (average Eu/Eu* = 0.85; Fig. 6d).

4.3. Zircon U-Pb age determinations

In BSE/CL images, zircon grains from the Tistronskär monzodiorite (sample A2274) show oscillatory zoning in rims with inherited cores, but some zircons are homogeneous and lack observable internal structures (Electronic Appendix B). Altogether, 22 spots from 22 zircon grains were analyzed using LA-ICP-MS. All the analyses are concordant and yield a concordia age of 1805 ± 4 Ma with an MSWD of concordance + equivalence 0.7, which we interpret as the crystallization age of the Tistronskär monzodiorite (Fig. 7a).

In BSE images, zircon grains from the Loukee granite (sample A2439) are rounded, euhedral, homogeneous and lack oscillatory zoning patterns (Electronic Appendix B). Altogether, 17 spots from 17 zircon grains were analyzed using LA-ICP-MS. The obtained results are mainly discordant and the $^{207}Pb/^{206}Pb$ ages vary from 1481 to 1853 Ma. The analyzed spots have Th/U ratios varying from 0.08 to 0.48, which are typical for igneous zircons (Rubatto 2002). The most discordant analyses are from U-enriched zircons (U = 1345−2090 ppm). One spot deviating from the main population shows an older $^{207}Pb/^{206}Pb$ age of 1853 Ma and is excluded as an outlier indicating assimilation of older rock. The remaining 16 analyses define an upper intercept age of 1794 ± 13 Ma (MSWD = 5.9, Fig. 7b), which we interpret as the crystallization age of the Loukee granite.

4.4. Sm-Nd and Sr-Rb isotope geology

Sample GBTIST of the Tistronskär monzodiorite (from the same outcrop area as sample A2274 that was dated with the U-Pb method) was analyzed for whole-rock Sm-Nd and Sr-Rb isotopes (Table 1). The Tistronskär monzodiorite has a near-chondritic initial εNd value of -0.4 ± 0.4 (at 1805 Ma) and a depleted mantle model age of 2060 Ma. The $^{147}Sm/^{144}Nd$ value is very low (0.0843) compared to the present-day chondritic value of 0.1966 (Jacobsen & Wasserburg 1984). The sample has a relatively low Rb content (104 ppm) and high Sr content (2064 ppm) and thus the $^{87}Rb/^{86}Sr$ ratio is low (0.1455). The measured $^{87}Sr/^{86}Sr$ ratio is 0.706937, and the calculated initial $^{87}Sr/^{86}Sr$ ratio is 0.70322 ± 0.00007. The initial $^{87}Sr/^{86}Sr$ ratio is somewhat higher than that of the Uniform Reservoir at 1.80 Ga (0.7024; Faure 2001).

Table 1. Whole-rock Nd and Sr isotope composition of the 1805 Ma Tistronskär monzodiorite.

Sample field code	GBTIST
Sm (ppm)	23.1
Nd (ppm)	165.5
$^{147}Sm/^{144}Nd$	0.08434
$^{143}Nd/^{144}Nd$ [a]	0.511290 ± 0.000006
εNd_i (at 1805 Ma) [b]	-0.4 ± 0.4
T_{DM} (Ma) [c]	2060
Rb (ppm)	103.8
Sr (ppm)	2063.7
$^{87}Rb/^{86}Sr$	0.1455
$^{87}Sr/^{86}Sr$ [a]	0.706937 ± 0.000014
$^{87}Sr/^{86}Sr_i$ (at 1805 Ma) [d]	0.70322 ± 0.00007

Note: Isotopic analyses at the Geological Survey of Finland by the last author.
[a] $^{143}Nd/^{144}Nd$ normalized to $^{146}Nd/^{144}Nd$ = 0.7219, $^{87}Sr/^{86}Sr$ normalized to $^{87}Sr/^{88}Sr$ = 0.1194; reported errors are 2σ.
[b] Initial Nd isotope composition expressed as the εNd value, calculated using $\lambda^{147}Sm = 6.524\times10^{-12} a^{-1}$, $^{147}Sm/^{144}Nd$ = 0.1966 and $^{143}Nd/^{144}Nd$ = 0.512638.
[c] Depleted mantle model age after DePaolo (1981).
[d] Initial Sr isotope composition, with external 2σ error indicated, calculated using $\lambda^{87}Rb = 1.3972\times10^{-11} a^{-1}$ of Villa et al. (2015).

5. Discussion

5.1. *Petrogenesis of Tistronskär monzodiorite*

New age data for the Tistronskär monzodiorite yielded a U-Pb zircon age of 1805 ± 4 Ma (Fig. 7a). Thus, the monzodiorite is coeval with post-orogenic intrusions elsewhere in the Svecofennian province. Moreover, the monzodiorite shows the same geochemical characteristics (high K, P, Ti, Ba, Sr and LREE) as the basic/intermediate post-orogenic rocks (Fig. 6c). As a result, we suggest that Tistronskär is a post-orogenic intrusion.

In both the SFS and Russian Karelia, basic post-orogenic rocks are suggested to have their sources in the subcontinental lithospheric mantle, which was enriched during the Svecofennian orogeny (Väisänen et al. 2000, Andersson et al. 2006). The post-orogenic rocks have relatively restricted radiogenic isotope ratios (initial Sr = 0.7019 to 0.7035 and εNd (t) = +1.4 to -0.8) and broadly similar primitive mantle-normalized trace element patterns (Figs. 6 and 8). This strongly suggests that these post-orogenic rocks were derived from similar sources and reflect similar magmatic processes. The Tistronskär monzodiorite initial Sr value (0.7032) and εNd value (-0.4) plots between these ranges (Fig. 8). This indicates that the Tistronskär monzodiorite could have been derived from sources similar to those of the other post-orogenic rocks.

Eklund et al. (1998) suggested that magmas derived from subduction-influenced carbonated mantle could explain high Ba-Sr signatures in post-orogenic rocks since the enriched LREE and LILE characters could have been inherited from subducted sediment and carbonate melts. In addition, Woodard & Huhma (2015) suggested that metasomatic enrichment of the lithospheric mantle occurred as a two-stage process. First, in an active subduction stage (>1.87 Ga), amphibole- and phlogopite-rich veins crystallized in the mantle from a hydrous alkaline silicate melt, formed as a consequence of melting of the subducted sediments. They added that silicate melt, with high Rb/Sr and $^{87}Sr/^{86}Sr$ would control the $^{87}Sr/^{86}Sr$ characteristics of the enriched mantle source. The second metasomatism occurred during a post-orogenic thermal re-equilibration where the mantle melting led to further melting of the subducted sediments, producing carbonatitic melt, which was filtrated preferentially into the vein network. Carbonatite melt (LREE enriched, low Sm/Nd) would control the $^{143}Nd/^{144}Nd$ characteristics (Woodard & Huhma 2015). Metasomatic enrichment is also supported by experimental studies (Wyllie & Sekine 1982; Förster et al. 2019), as it has illustrated

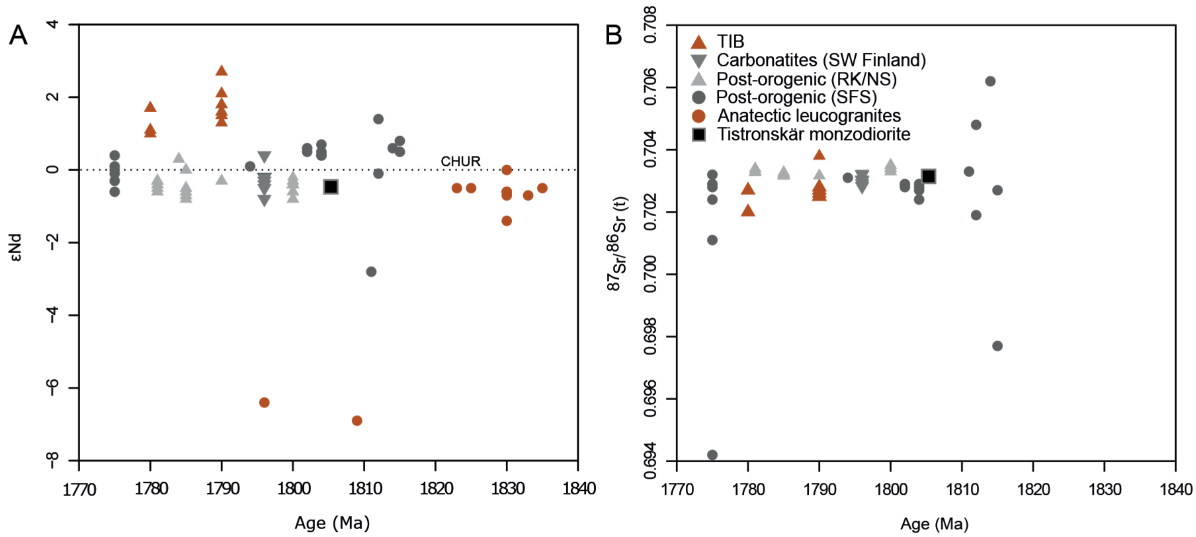

Fig. 8. Age versus Nd and Sr diagrams showing the initial Nd and Sr isotope composition of the Tistronskär monzodiorite dated by the U-Pb method in this study. Also shown is the composition of the 46 previously analysed post-orogenic basic to acidic intrusions from the Southern Finland Subprovince (SFS), North Savo (NS) and Russian Karelia (RK) (Patchett & Kouvo 1986; Lahtinen & Huhma 1997; Eklund et al. 1998; Konopelko et al. 2005; Andersson et al. 2006; Rutanen et al. 2011; Woodard & Huhma 2015), 11 anatectic leucogranites from SFS (Huhma 1986; Kurhila et al. 2005, 2011) and 10 basic plutonic rocks from Transscandinavian Igneous Belt (TIB) (Rutanen & Andersson 2009). CHUR is chondritic uniform reservoir (DePaolo & Wasserburg 1976).

that amphibole- and phlogopite-bearing pyroxenite can be produced by addition of melts from subducted sediments interacting with depleted mantle regions. Geochemically comparable melts to the basic post-orogenic shoshonitic rocks in the SFS have been shown to be equilibrium with phlogopite pyroxenite assemblages (Becerra-Torres et al. 2020). In addition, the 1.80 Ga monzodiorite has a low SiO_2 content (49.8–53.9 wt.%) and relatively high Mg# (60–65), indicating that their parental magmas were predominantly mantle derived. Moreover, a high P_2O_5 content (up to 2.92 wt.%) and P_2O_5/TiO_2 ratio (up to 1.63) of the Tistronskär monzodiorite is consistent with a magma source modified by carbonatite melt metasomatism (e.g., Baker & Wyllie 1992). It is suggested that differences in carbonate metasomatism may explain the regional geochemical differences, so that the source of the rocks in Russian Karelia were more affected by carbonate metasomatism (Eklund et al. 1998; Andersson et al. 2006). As shown in Figure 9a, post-orogenic rocks from Russian Karelia and North Savo show higher Ce/Yb and P_2O_5/TiO_2 ratios than post-orogenic rocks from the SFS. The Tistronskär monzodiorite shows a similar Ce/Yb and P_2O_5/TiO_2 ratios than the SFS post-orogenic rocks (Fig. 9a). In the SiO_2 versus Rb/Ba diagram (Fig. 9b) Tistronskär monzodiorite shows a similar Rb/Ba < 0.1 character to other post-orogenic rocks. This indicates that the Tistronskär monzodiorite is similar to the post-orogenic rocks in the SFS but differs from rocks situated in Russian Karelia, where carbonate metasomatism has been stronger (Eklund et al. 1998).

In subduction zones, the subcontinental mantle can be enriched by sediment derived aqueous fluids or melts, carbonate derived fluids/melts, or melts from altered oceanic crust (Spandler & Pirard 2013). It is unclear what the proportion of sediment versus carbonate enrichment is, but some conclusions can be drawn from geochemical comparisons with other rock types. The primitive mantle-normalized trace element pattern of the Tistronskär monzodiorite is generally similar to GLOSS (global subducting sediments; Plank 2014), suggesting that the mantle was metasomatized

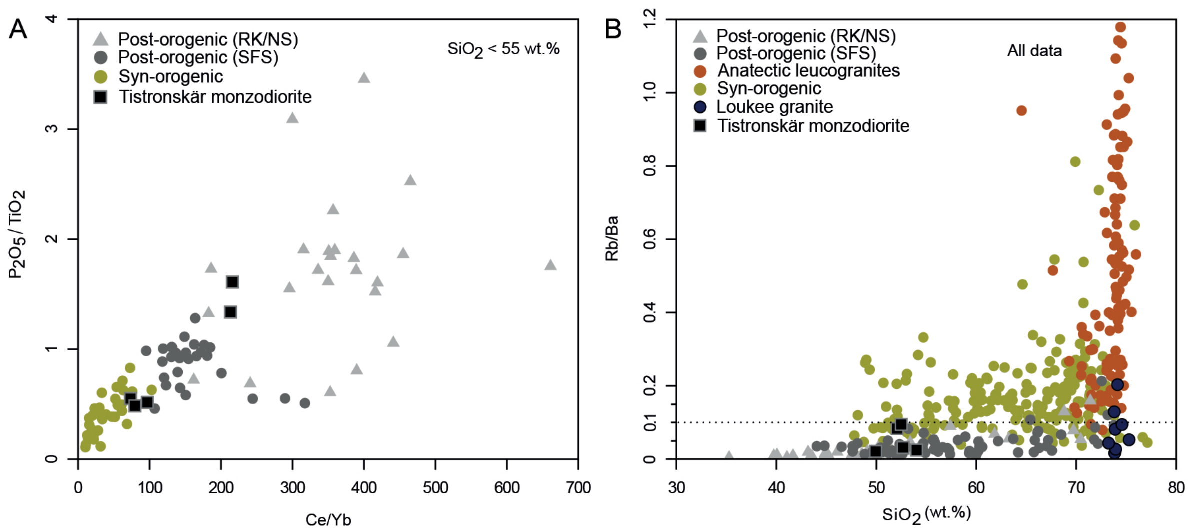

Fig. 9. Tistronskär monzodiorite and Loukee granite compared to other plutonic rocks from Southern Finland Subprovince (SFS), North Savo (NS) and Russian Karelia (RK). a) Ce/Yb versus P_2O_5/TiO_2 for basic rocks (SiO_2 < 55 wt.%). b) SiO_2 versus Rb/Ba for all rocks.

by subducted sediment derived melts (Fig. 10a). Subducted sediment derived melts can enrich the mantle source with elements such as K, Ba, Sr, LREE, Ti, Th and Zr (Hermann & Rubatto 2009; Turner & Langmuir 2022). These values are higher in Tistronskär monzodiorite and other post-orogenic intrusions than those of the 1.88−1.87 Ga syn-orogenic basic metavolcanic and plutonic rocks in the WFS (Fig. 10b). The sediment melt is inferred here because Th is strongly soluble in hydrous silicate melts (Johnson & Plank 1999; Kessel et al. 2005; Spandler & Pirard 2013), and the Tistronskär monzodiorite has Th values higher than those of the 1.88−1.87 Ga basic metavolcanic and plutonic rocks in the WFS (Fig. 10b). Furthermore, studies by Spandler et al. (2007) and Hermann & Rubatto (2009) have shown that sediment derived aqueous fluids cannot produce the same high Ba, Sr and LREE characteristics as observed in Tistronskär monzodiorite. Moreover, sediment derived melts are suggested here because melts from altered oceanic crust are not sufficiently enriched in incompatible elements (K, Ba, Sr, Rb and Th) to be a possible source of enrichment for Tistronskär monzodiorite, as demonstrated in Figure 10a. In addition, even if the altered oceanic crust melted in the mantle regions, it is too isotopically depleted to explain the initial $^{87}Sr/^{86}Sr$ isotopic composition of the Tistronskär monzodiorite. We conclude that the origin of the Tistronskär monzodiorite is related to an enriched mantle source. The mantle source might have been metasomatized by melts derived from terrigenous sediments (LREE, Th, Zr, Ti and $^{87}Sr/^{86}Sr$ increase) and from CO_2-rich melts/fluids (P_2O_5, Ba, Th, Sr and LREE increase), which promoted the upper mantle to melt at the post-orogenic stage.

5.2. Petrogenesis of Loukee HiBaSr granite

The composition of the granitic dykes from Loukee is characterized by high Ba and Sr contents, and negative Nb and Ta anomalies (Figs. 6c and 11a). They are similar to high Ba-Sr (HiBaSr) granitoids worldwide and thus distinct from the more common I-, S- and A-type granites (Tarney & Jones 1994; Lara et al. 2017). These HiBaSr granitoids are also distinct from adakites in having more variable Y and Yb contents and higher Ba/Sr and K_2O/Na_2O ratios (e.g., Kara et al. 2020). Thus, the Loukee granite is regarded as a high Ba-Sr granitoid.

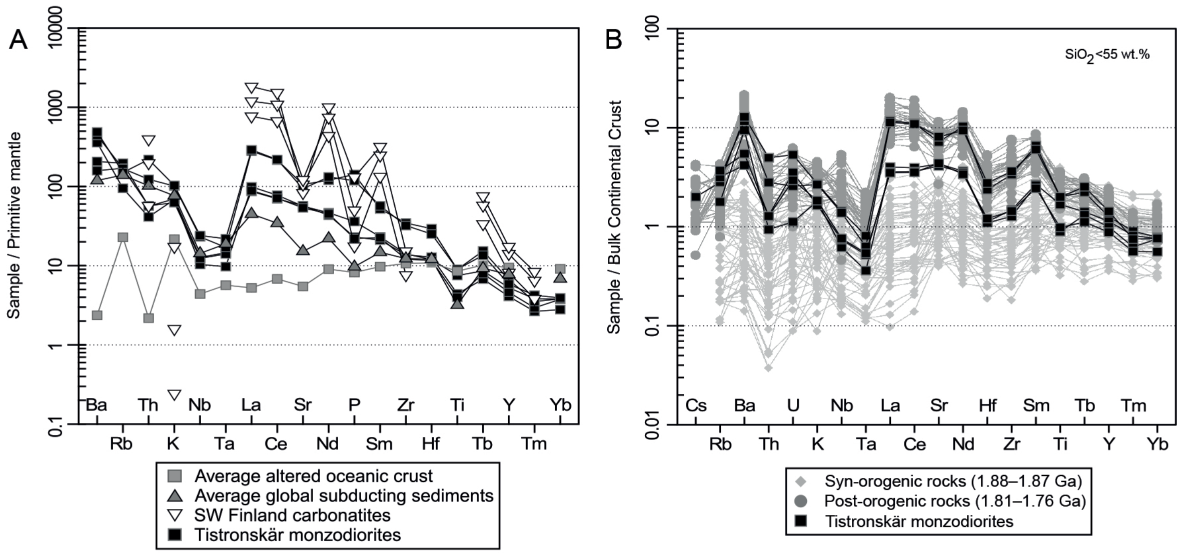

Fig. 10. a) Tistronskär monzodiorite (this study and data from Lehtonen et al. 2003) compared to average altered oceanic crust (Kelley et al. 2003), average global subducting sediments (Plank 2014) and carbonatites from southwest Finland (Woodard & Hölttä 2005) in a multi-element plot normalized to primitive mantle after McDonough & Sun (1995). b) Tistronskär monzodiorite compared to the syn-orogenic metavolcanic and plutonic rocks (SiO_2 < 55 wt.%) from the Western Finland Subprovince and post-orogenic rocks (SiO_2 < 55 wt.%) from the Southern Finland Subprovince (Electronic Appendix A) in multi-element plot normalized to bulk continental crust after Taylor and McLennan (1995). All the 1.88–1.87 Ga syn-orogenic metavolcanic and plutonic rocks (Lehtonen et al. 2003; Geological Survey of Finland 2014) are from the schist belts that encircles the Central Finland Granitoids Complex from Tampere to the NW to the Ostrobothnian Schist Belt.

Post-orogenic HiBaSr granitoids with similar geochemical characteristics (high K, P, Ti, Ba, Sr and LREE) and crystallization ages (~1.80 Ga) as the Loukee HiBaSr granite have been described throughout the SFS (Rutanen et al. 2011). These acidic rocks can be distinguished from the 1.90−1.88 Ga syn-orogenic acidic plutonic rocks and anatectic leucogranites in Ba-Sr content (Fig. 11a) and Sr-Rb-Ba ratio (Fig. 11b). New age data on the Loukee granite yielded a U-Pb zircon age of 1794 ± 13 Ma (Fig. 7b). As a result, we suggest that Loukee granite is a post-orogenic intrusion.

Eklund et al. (1998) and Andersson et al. (2006) suggested that post-orogenic HiBaSr granitic rocks are clearly mantle derived and therefore the characteristic chemistry of this granitoid group must be defined by the mantle source rather than the crustal source. The same geochemical, chronological and isotopic characteristics of the post-orogenic rocks (lamprophyres, monzogabbros, monzonites and HiBaSr granites) in the SFS indicate a common/similar source (Eklund et al. 1998). Intermediate-acidic rocks from the SFS are closely associated with coeval basic rocks and are suggested to have been formed by the extensive fractionation of mantle-derived shoshonitic melts (Eklund et al. 1998). Our interpretation is that Loukee granite was also formed by fractional crystallization from basic/intermediate shoshonitic melts, as Loukee granite shows the same geochemical characteristics as the other acidic post-orogenic rocks in the SFS (Fig. 6).

Regarding the lower crustal melting origin for the HiBaSr granites, experimental studies have shown that the melting of amphibolites and basalts with/without fractional crystallization could produce granitic magmas (Beard & Lofgren 1991; Sisson et al. 2005; Blatter et al. 2013; Nandedkar et al. 2014; Palin et al. 2016). These studies show that

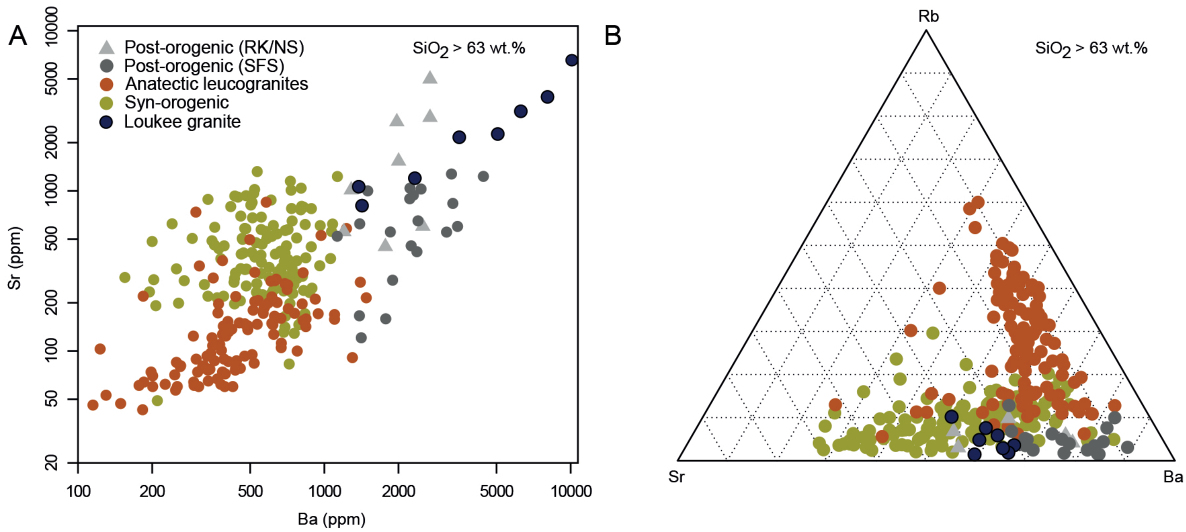

Fig. 11. Loukee granite compared to other acidic plutonic rocks from the Southern Finland Subprovince (SFS), North Savo (NS) and Russian Karelia (RK). a) Ba-Sr binary diagram. b) Sr-Rb-Ba ternary diagram.

melts from amphibolites and basalts are strongly peraluminous, rich in Al_2O_3 and CaO, and poor in K_2O, following the calc-alkaline magma series. The HiBaSr granites have relatively low values of Al_2O_3 and CaO, high K_2O, and are mostly metaluminous, following the shoshonitic magma series. Moreover, the near-chondritic initial εNd values from the post-orogenic acidic rocks (0.6 to -0.6; Rutanen et al. 2011) indicates that their petrogenesis differs from that of anatectic leucogranites throughout the SFS. As anatectic leucogranites show lower initial εNd values (-0.5 to -1.4; Fig. 8a), where a range of metaigneous and metasedimentary rocks have been suggested involved in their petrogenesis (Kurhila et al. 2011). Therefore, basalt and amphibolite are unlikely to be sources of the HiBaSr granites.

5.3. Petrogenetic interpretation for shoshonitic magmatism in the WFS and SFS

Possible explanations for the melt formation in the mantle in post-orogenic settings in the WFS and SFS are related to the upwelling of hot asthenospheric material caused by plume activity (Peltonen et al. 2000), convective thinning of the lithosphere (Väisänen et al. 2000), slab break-off event (Eklund & Shebanov 2002; Saalmann et al. 2009), delamination (Kosunen 2004), gravitational collapse enhanced by lithospheric delamination (Korja et al. 2006) or decay of radioactive isotopes (Kukkonen & Lauri 2009). Both the Tistronskär and Loukee intrusions show mantle source affinities, thus were likely formed primarily by mantle melts. The ages from different post-orogenic shoshonitic intrusions in the SFS span over at least 55 Ma (from 1815 Ma to 1760 Ma, although most ages cluster around 1800 Ma) suggesting that a protracted, diachronous, and probably multistage process gave rise to shoshonitic magmatism within a post-orogenic setting (Väisänen et al. 2000; Eklund & Shebanov 2005). Despite the range in magmatic ages, these intrusions are similar in petrological character and geochemical composition, suggesting that they share a common source and petrogenesis (Rutanen et al. 2011). Thus, these shoshonitic melts are considered to form by long-lasting event that has operated in the WFS and SFS, starting at 1815 Ma, forming the peak at 1800 Ma and lasting all the way to 1760 Ma. Thus, viable petrogenetic models must account the long-lasting mantle melting in the WFS and SFS.

Juvenile crust formation during the arc-continent collision between the tectonic blocks represented by the Svecofennia and Karelia provinces was accompanied by thickening of the lithosphere. Korja et al. (1993) proposed that, after collision, the lithosphere may be thinned by delamination. This could be one long-lasting mechanism for producing heat additions to the base of the crust and causing melting of both the upper mantle and lower crust in a post-orogenic setting. During the formation of 1.84−1.82 Ga anatectic leucogranites in the SFS, in which granitic plutons compose most of the upper crust (Fig. 2), there must be a complementary production of a thick, deeper section of mafic garnet granulites that form as residues of the granitoids. This is seen in large-scale seismic array studies of the lower crust across the SFS, which show a thinner high P-wave velocity layer underneath the SFS compared to the thicker high-velocity layers further north (Yliniemi et al. 2004). Areas of high-velocity lower crust are interpreted to consist of a mixture of hornblendites, mafic garnet granulites, pyroxenites and mafic eclogites (Kuusisto et al. 2006). In addition, Janik et al. (2007) interpreted the seismic data to indicate that in the SFS, the lower crust is eclogitic compared to the mafic garnet granulite lower crust further north. Another characteristic feature of the SFS is that the crust is more than 10 km thinner than further north, which is interpreted in terms of thinning after the thickening process (Korja et al. 1993). Moreover, post-orogenic intrusions seem to appear everywhere, except in areas where crustal thicknesses exceed 56 km (Korja et al. 1993; Yliniemi et al. 2004). Furthermore, melting of mafic metavolcanic rocks could generate dense mafic garnet granulite residues in the lower crust, as modeled by Andersen & Rämö (2021). The availability of hydrous fluids (e.g., from a nearby subducting plate, TIB magmatism, Fig. 1) could facilitate lower crust eclogitization (Krystopowicz & Currie 2013). This eclogite phase change itself induces lower crustal weakening and could initiate lower crust delamination in the WFS and SFS. This is consistent with the notion that a phase transformation in the lower crust from mafic granulite to eclogite plays a major role in the development of delamination (Meissner & Mooney 1998; Krystopowicz & Currie 2013). Thus, lower crust/upper mantle delamination, seems to be a possible scenario to account the post-orogenic magmatism across the WSF and SFS, but only in the parts where the crust is thinner than 56 km.

On the scale of the entire Svecofennian province, the 1.89–1.87 Ga magmatic episode has been related to N-S directed shortening, amalgamation of island arcs, and regional deformation (Chopin et al. 2020; Lahtinen et al. 2023). In contrast, the post-orogenic magmatic episode in 1.81–1.76 Ga was characterized by shifts in plate convergence (transpressional shearing) and by a diversity of magmatic suites, including suites derived from the subcontinental mantle and widespread granitoid rocks extracted from the continental crust (Fig. 1; Ehlers et al. 1993; Eklund et al. 1998; Heilimo et al. 2014). The diversity of concurrent magmatic events across the Svecofennian province and the temporal coincidence with active TIB magmatism in the west suggest that transpressional shearing related to the TIB magmatism has affected the juvenile Svecofennian continent and may have reached through the whole lithosphere (Andersson et al. 2006). Thus, there may be a link between the availability of hydrous fluids (e.g., from a nearby subducting plate), lower crust eclogitization, and delamination (Fig. 12).

Many authors have proposed that TIB magmatism can be genetically linked to the widespread post-orogenic magmatism occurring in a whole Svecofennian province (Nironen 1997; Korja et al. 1993; Pesonen 2003; Andersson et al. 2006; Heilimo et al. 2014; see Fig. 1), and related mafic underplating may also form a large subsurface mafic intrusion underneath the Svecofennian province as well (Väisänen et al. 2000; Woodard et al. 2014). The 1.80 Ga zircons from mantle and lower crustal xenoliths in eastern Finland verify this large-scale mantle activity at this time (Hölttä et al. 2000; Peltonen & Mänttäri 2001). We suggest

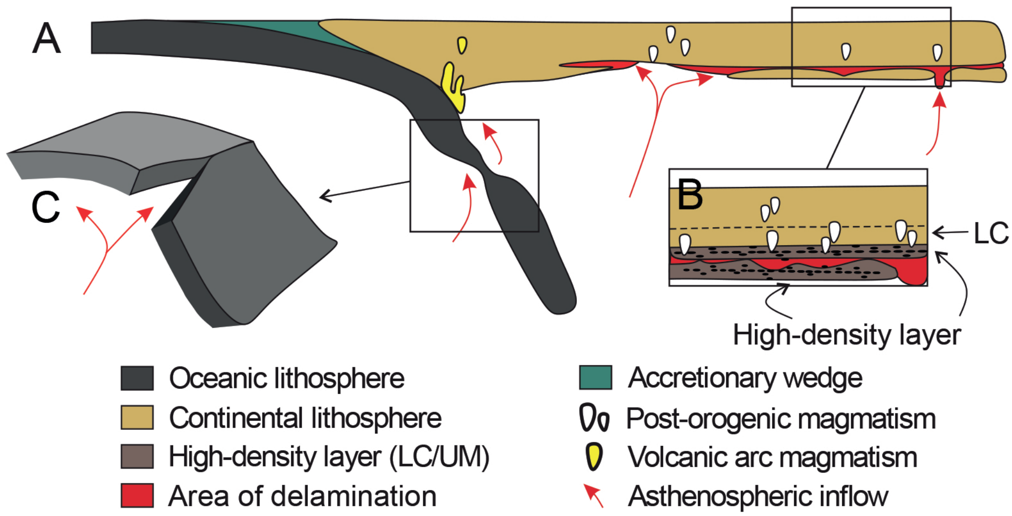

Fig. 12. Schematic model of the generation of post-orogenic magmas: Post-orogenic magmas form as a result of delamination and partial slab break-off in the thickened lithosphere created by the Svecofennian orogeny. A) Drip-type delamination occurs in the heterogenous high-density layer of lower crust and upper mantle. This delamination allows asthenospheric inflow, providing the necessary heat and causing melting of both the upper mantle and lower crust. B) The high-density layer is compositionally heterogeneous and enriched with various components during the Svecofennian orogeny. C) Partial slab break-off, or slab tearing, could also cause localized asthenospheric influx, leading to melting. LC = lower crust and UM = upper mantle.

that the combination of the high-density layer foundering to the upper mantle and the slab break-off/rollback event triggered upper mantle melting in the WFS and SFS (Fig. 12). This setting explains the debated heat source as well as the occurrence of high Ce/Yb shoshonitic magmatism in Russian Karelia (Fig. 9a), which is interpreted to have formed deeper in the lithosphere than shoshonitic intrusions closer to the TIB (Andersson et al. 2006). In this context, the WFS, SFS and Russian Karelia represent the distal intracontinental regions from the newly formed active continental margin in the west (Figs. 1 and 12). In this scenario, delamination of the overthickened crust occurred far from the active continental margin. This could have caused new heat flow and mafic underplating of the continental crust, giving rise to melt production and post-orogenic magmatic activity in the central part of the craton. The delamination process suggested here is drip-type, as proposed by Houseman & Molnar (1997), meaning that the high-density layer delaminates only partially. We suggest that a small-scale drip-like delamination within the crust-mantle boundary was necessary to form widespread shoshonitic intrusions in the WFS and SFS. At the time of the generation of post-orogenic magmas, the active continental margin was located around the current border between Sweden and Norway, where subduction produced volcanic arc magmatism and formed the Transscandinavian Igneous Belt.

6. Conclusions

We have characterized the geochemistry, age and whole-rock Sr-Nd isotope composition of the Tistronskär LREE-rich monzodiorite and the geochemistry and age of the Loukee high Ba-Sr granite in western and southern Finland. The main results are:

1) The zircon U-Pb age of the Tistronskär monzodiorite is 1805 ± 4 Ma and that of the Loukee granite is 1794 ± 13 Ma.

2) The Tistronskär monzodiorite and Loukee granite can be classified as HiBaSr shoshonitic intrusions.

3) The ages (~1.80 Ga) from Tistronskär monzodiorite and Loukee granite indicate that they can be classified as post-orogenic intrusions.

4) Tistronskär monzodiorite and Loukee granite show the same enriched geochemical characteristics (high K, P, Ti, Ba, Sr, LREE) as the other post-orogenic intrusions in the SFS.

5) The slab break-off model combined with lower crust delamination is suggested to have been responsible for upper mantle melting to generate shoshonitic melts in the WSF and SFS. It is suggested that the crystallization of carbonatite melts in the upper mantle and the subsequent release of CO_2-H_2O-rich fluids could possibly induce the melting of phlogopite pyroxenites in the upper mantle.

Acknowledgments

This study was funded by K.H. Renlund Foundation (O. Teräs) and the MIDCRUST consortium (Dr. Anna-Kaisa Korja, P.I.; Prof. O.T. Rämö, co-P.I.; Academy of Finland project 139035). GTK laboratory and Dr. Hannu Huhma are thanked for providing Loukee granite U-Pb analysis. Editor Jarmo Kohonen and reviewers Dmitri Konopelko and Jeremy Woodard are thanked for their constructive comments which all helped to improve the manuscript.

Supplementary Data

Electronic Appendices are available via Bulletin of the Geological Society Finland web page.
Electronic Appendix A: Whole-rock geochemical analyses and post-orogenic reference dataset.
Electronic Appendix B: Zircon U-Pb LA-ICP-MS analyses and zircon BSE images/descriptions.

References

Ahtonen, N., Hölttä, P. & Huhma, H., 2007. Intracratonic Palaeoproterozoic granitoids in northern Finland: Prolonged and episodic crustal melting events revealed by Nd isotopes and U-Pb ages on zircon. Bulletin of the Geological Society of Finland 79, 143–174. https://doi.org/10.17741/bgsf/79.2.002

Alviola, R., Mänttäri, I., Mäkitie, H. & Vaasjoki, M., 2001. Svecofennian rare-element granitic pegmatites of the Ostrobothnia region, western Finland; their metamorphic environment and time of intrusion. Geological Survey of Finland, Special Paper 30, 9–29. https://tupa.gtk.fi/julkaisu/specialpaper/sp_030.pdf

Andersen, T. & Rämö, O. T., 2021. Dehydration Melting and Proterozoic Granite Petrogenesis in a Collisional Orogen—A Case from the Svecofennian of Southern Finland. Journal of Earth Science 32, 1289–1299. https://doi.org/10.1007/s12583-020-1385-8

Andersson, U. B., Eklund, O., Fröjdö, S. & Konopelko, D., 2006. 1.8 Ga magmatism in the Fennoscandian Shield; lateral variations in subcontinental mantle enrichment. Lithos 86, 110–136. https://doi.org/10.1016/j.lithos.2005.04.001

Atherton, M. P. & Ghani, A. A., 2002. Slab breakoff: A model for Caledonian, Late Granite syn-collisional magmatism in the orthotectonic (metamorphic) zone of Scotland and Donegal, Ireland. Lithos 62, 65–85. https://doi.org/10.1016/S0024-4937(02)00111-1

Baker, M. B. & Wyllie, P. J., 1992. High-pressure apatite solubility in carbonate-rich liquids: Implications for mantle metasomatism. Geochimica et Cosmochimica Acta 56, 3409–3422. https://doi.org/10.1016/0016-7037(92)90388-Y

Beard, J. S. & Lofgren, G. E., 1991. Dehydration Melting and Water-Saturated Melting of Basaltic and Andesitic Greenstones and Amphibolites at 1, 3, and 6. 9 kb. Journal of Petrology 32, 365–401. https://doi.org/10.1093/petrology/32.2.365

Becerra-Torres, E., Melekhova, E., Blundy, J. D. & Brooker, R. A., 2020. Experimental evidence for decompression melting of metasomatized mantle beneath Colima Graben, Mexico. Contributions to Mineralogy and Petrology 175, 1–21. https://doi.org/10.1007/s00410-020-01740-x

Bergman, S., Högdahl, K., Nironen, M., Ogenhall, E., Sjöström, H., Lundqvist, L. & Lahtinen, R., 2008. Timing of Palaeoproterozoic intra-orogenic sedimentation in the central Fennoscandian Shield; evidence from detrital zircon in metasandstone. Precambrian Research 161, 231–249. https://doi.org/10.1016/j.precamres.2007.08.007

Blatter, D. L., Sisson, T. W. & Hankins, W. B., 2013. Crystallization of oxidized, moderately hydrous arc basalt at mid- to lower-crustal pressures: Implications

for andesite genesis. Contributions to Mineralogy and Petrology 166, 861–886. https://doi.org/10.1007/s00410-013-0920-3
Bonin, B., 2004. Do coeval mafic and felsic magmas in post-collisional to within-plate regimes necessarily imply two contrasting, mantle and crustal, sources? A review. Lithos 78, 1–24. https://doi.org/10.1016/j.lithos.2004.04.042
Bonin, B., Azzouni-Sekkal, A., Bussy, F. & Ferrag, S., 1998. Alkali-calcic and alkaline post-orogenic (PO) granite magmatism: Petrologic constraints and geodynamic settings. Lithos 45, 45–70. https://doi.org/10.1016/S0024-4937(98)00025-5
Branigan, N. P., 1987. The geology, geochemistry and tectonic setting of the early-postorogenic ring complexes, Åland, SW Finland. PhD thesis, University of Dundee, Scotland, 586 p.
Chappell, B. W. & White, A. J. R., 2001. Two contrasting granite types: 25 years later. Australian Journal of Earth Sciences 48, 489–499. https://doi.org/10.1046/j.1440-0952.2001.00882.x
Choi, S. G., Rajesh, V. J., Seo, J., Park, J. W., Oh, C. W., Pak, S. J. & Kim, S. W., 2009. Petrology, geochronology and tectonic implications of Mesozoic high Ba–Sr granites in the Haemi area, Hongseong Belt, South Korea. Island Arc 18, 266–281. https://doi.org/10.1111/j.1440-1738.2008.00622.x
Chopin, F., Korja, A., Nikkilä, K., Hölttä, P., Korja, T., Abdel Zaher, M., Kurhila, M., Eklund, O. & Rämö, O. T., 2020. The Vaasa Migmatitic Complex (Svecofennian Orogen, Finland): Buildup of a LP-HT Dome During Nuna Assembly. Tectonics 39, e2019TC005583. https://doi.org/10.1029/2019TC005583
Clemens, J. D., Bryan, S. E., Mayne, M. J., Stevens, G. & Petford, N., 2022. How are silicic volcanic and plutonic systems related? Part 1: A review of geological and geophysical observations, and insights from igneous rock chemistry. Earth-Science Reviews 235, 104249. https://doi.org/10.1016/j.earscirev.2022.104249
Condamine, P. & Médard, E., 2014. Experimental melting of phlogopite-bearing mantle at 1 GPa: Implications for potassic magmatism. Earth and Planetary Science Letters 397, 80–92. https://doi.org/10.1016/j.epsl.2014.04.027
Couzinié, S., Laurent, O., Moyen, J. F., Zeh, A., Bouilhol, P. & Villaros, A., 2016. Post-collisional magmatism: Crustal growth not identified by zircon Hf–O isotopes. Earth and Planetary Science Letters 456, 182–195. https://doi.org/10.1016/j.epsl.2016.09.033
DePaolo, D. J., 1981. Neodymium isotopes in the Colorado Front Range and crust–mantle evolution in the Proterozoic. Nature 291, 193–196. https://doi.org/10.1038/291193a0
DePaolo, D. J. & Wasserburg, G. J., 1976. Inferences about magma sources and mantle structure from variations of 143Nd/144Nd. Geophysical Research Letters 3, 743–746. https://doi.org/10.1029/GL003i012p00743
Duchesne, J. C., Berza, T., Liégeois, J. P. & Vander Auwera, J., 1998. Shoshonitic liquid line of descent from diorite to granite: The Late Precambrian post-collisional Tismana pluton (South Carpathians, Romania). Lithos 45, 281–303. https://doi.org/10.1016/S0024-4937(98)00036-X
Ehlers, C., Lindroos, A. & Selonen, O., 1993. The late Svecofennian granite-migmatite zone of southern Finland—A belt of transpressive deformation and granite emplacement. Precambrian Research 64, 295–309. https://doi.org/10.1016/0301-9268(93)90083-E
Eklund, O., Konopelko, D., Rutanen, H., Fröjdö, S. & Shebanov, A. D., 1998. 1.8 Ga Svecofennian post-collisional shoshonitic magmatism in the Fennoscandian shield. Lithos 45, 87–108. https://doi.org/10.1016/S0024-4937(98)00027-9
Eklund, O. & Shebanov, A. D., 2002. A Slab Breakoff Model for the Differentiation of the Svecofennian Crust in Southern Finland. In: Lahtinen, R. et al. (eds.), Proceedings of the 2th Symposium on the Structure, Composition and Evolution of the Lithosphere in Finland. Espoo, Finland, pp. 9−13. https://www.seismo.helsinki.fi/pdf/Lito2002.pdf
Eklund, O. & Shebanov, A. D., 2005. Prolonged postcollisional shoshonitic magmatism in the southern Svecofennian domain–a case study of the Åva granite–lamprophyre ring complex. Lithos 80, 229−247. https://doi.org/10.1016/j.lithos.2004.06.012.
Eklund, O. & Fröjdö, S., 2012. Petrology of an enriched gabbro in the Bothnian core complex. In: Kukkonen, I. et al. (eds.), Proceedings of the 7th Symposium on the Structure, Composition and Evolution of the Lithosphere in Finland. Espoo, Finland, pp. 13−15. https://www.seismo.helsinki.fi/pdf/Lito2012.pdf
Faure, G., 2001. Origin of igneous rocks: The isotopic evidence. Heidelberg, Springer Berlin, 496 p. https://doi.org/10.1007/978-3-662-04474-2
Förster, M. W., Prelević, D., Buhre, S., Mertz-Kraus, R. & Foley, S. F., 2019. An experimental study of the role of partial melts of sediments versus mantle melts in the sources of potassic magmatism. Journal of Asian Earth Sciences 177, 76–88. https://doi.org/10.1016/j.jseaes.2019.03.014
Fowler, M. B., Kocks, H., Darbyshire, D. P. F. & Greenwood, P. B., 2008. Petrogenesis of high Ba–Sr plutons from the Northern Highlands Terrane of the British Caledonian Province. Lithos 105, 129–148. https://doi.org/10.1016/j.lithos.2008.03.003
Geological Survey of Finland, 2014. Spatial data products: Rock geochemical data of Finland. https://hakku.gtk.fi/en/locations/search [referred 11.12.2023].
Geological Survey of Finland, 2016. Spatial data products: Bedrock of Finland 1:1 00 000 and Aeromagnetic anomaly map of Finland. https://hakku.gtk.fi/en/locations/search [referred 11.12.2023].
Geological Survey of Finland, 2019. Spatial data products: Bedrock of Finland 1:5 000 000 / 1:10 000 000. https://hakku.gtk.fi/en/locations/search [referred 26.11.2024].
Geological Survey of Finland, 2022. Spatial data products: Bedrock of Finland 1:200 000. https://hakku.gtk.fi/en/locations/search [referred 11.12.2023].

Geological Survey of Norway, 2024. Geological maps: Data sets, BERGGRUNN N1350 (1:1.350.000). https://www.ngu.no/en/geologiske-kart/datasett [referred 4.3.2024].

Geological Survey of Sweden, 2022. Produkter och tjänster: GeoLagret, GE.Berggrund 1:1 miljon and Berget ålder isotopanalyser. https://apps.sgu.se/geolagret/ [referred 11.12.2023].

Gómez-Frutos, D., Castro, A. & Gutiérrez-Alonso, G., 2023. Post-collisional batholiths do contribute to continental growth. Earth and Planetary Science Letters 603, 117978. https://doi.org/10.1016/j.epsl.2022.117978

Heilimo, E., Ahven, M. & Mikkola, P., 2018. Geochemical characteristics of the plutonic rock units present at the southeastern boundary of the Central Finland Granitoid Complex. Geological Survey of Finland, Bulletin 407, 106–129. https://doi.org/10.30440/bt407.6

Heilimo, E., Elburg, M. A. & Andersen, T., 2014. Crustal growth and reworking during Lapland–Kola orogeny in northern Fennoscandia: U–Pb and Lu–Hf data from the Nattanen and Litsa–Aragub-type granites. Lithos 205, 112–126. https://doi.org/10.1016/j.lithos.2014.06.014

Heinonen, A. P., Rämö, O. T., Mänttäri, I., Andersen, T. & Larjamo, K., 2017. Zircon as a Proxy for the Magmatic Evolution of Proterozoic Ferroan Granites; the Wiborg Rapakivi Granite Batholith, SE Finland. Journal of Petrology 58, 2493–2517. https://doi.org/10.1093/petrology/egy014

Hermann, J. & Rubatto, D., 2009. Accessory phase control on the trace element signature of sediment melts in subduction zones. Chemical Geology 265, 512–526. https://doi.org/10.1016/j.chemgeo.2009.05.018

Hinchey, A. M., Sandeman, H. A. & Butler, J. P., 2023. The Paleoproterozoic granite factory: Voluminous post-collisional, ferroan, A-type granites and implications for crust formation and metallogenic tenor, Labrador, Canada. GSA Bulletin 136, 893–916. https://doi.org/10.1130/B36727.1

Högdahl, K., Andersson, U. B. & Eklund, O., 2004. The Transscandinavian Igneous Belt (TIB) in Sweden: A review of its character and evolution. Geological Survey of Finland, Special Paper 37, 1–123. https://tupa.gtk.fi/julkaisu/specialpaper/sp_037.pdf

Hölttä, P. & Heilimo, E., 2017. Metamorphic map of Finland. Geological Survey of Finland, Special Paper 60, 77–128. https://tupa.gtk.fi/julkaisu/specialpaper/sp_060_pages_077_128.pdf

Hölttä, P., Huhma, H., Mänttäri, I., Peltonen, P. & Juhanoja, J., 2000. Petrology and geochemistry of mafic granulite xenoliths from the Lahtojoki kimberlite pipe, eastern Finland. Lithos 51, 109–133. https://doi.org/10.1016/S0024-4937(99)00077-8

Houseman, G. A. & Molnar, P., 1997. Gravitational (Rayleigh–Taylor) instability of a layer with non-linear viscosity and convective thinning of continental lithosphere. Geophysical Journal International 128, 125–150. https://doi.org/10.1111/j.1365-246X.1997.tb04075.x

Hubbard, F. & Branigan, N., 1987. Late Svecofennian magmatism and tectonism, Åland, Southwest Finland. Precambrian Research 35, 241–256. https://doi.org/10.1016/0301-9268(87)90057-X

Huhma, H., Kousa, J. & Luukas, J., 2021. Geochronology of the Paleoproterozoic Pyhäsalmi–Vihanti district, central Finland. Geological Survey of Finland, GTK Open File Research Report 8/2021, 1–31. https://tupa.gtk.fi/raportti/arkisto/8_2021.pdf

Hyvönen, E., Airo, M.L, Arkimaa, H, Lerssi, J, Loukola-Ruskeeniemi, K, Vanne, J & Vuoriainen, S., 2013. Airborne geophysical, petrophysical and geochemical characteristics of Palaeoproterozoic black shale units in Finland: Applications for exploration and environmental studies. Geological Survey of Finland, Report of investigation 198, 58–60. https://tupa.gtk.fi/julkaisu/tutkimusraportti/tr_198.pdf

Jacobsen, S. B. & Wasserburg, G. J., 1984. Sm-Nd isotopic evolution of chondrites and achondrites, II. Earth and Planetary Science Letters 67, 137–150. https://doi.org/10.1016/0012-821X(84)90109-2

Janik, T., Kozlovskaya, E. & Yliniemi, J., 2007. Crust-mantle boundary in the central Fennoscandian shield: Constraints from wide-angle P and S wave velocity models and new results of reflection profiling in Finland. Journal of Geophysical Research: Solid Earth 112, B04302. https://doi.org/10.1029/2006JB004681

Jiang, Y. H., Liu, Z., Jia, R. Y., Liao, S. Y., Zhou, Q. & Zhao, P., 2012. Miocene potassic granite–syenite association in western Tibetan Plateau: Implications for shoshonitic and high Ba–Sr granite genesis. Lithos 134, 146–162. https://doi.org/10.1016/j.lithos.2011.12.012

Johansson, Å., Bingen, B., Huhma, H., Waight, T., Vestergaard, R., Soesoo, A., Skridlaite, G., Krzeminska, E., Shumlyanskyy, L., Holland, M. E., et al., 2022. A geochronological review of magmatism along the external margin of Columbia and in the Grenville-age orogens forming the core of Rodinia. Precambrian Research 371, 106463. https://doi.org/10.1016/j.precamres.2021.106463

Johnson, M. C. & Plank, T., 1999. Dehydration and melting experiments constrain the fate of subducted sediments. Geochemistry, Geophysics, Geosystems 1, 1–26. https://doi.org/10.1029/1999GC000014

Kähkönen, Y., 2005. Svecofennian supracrustal rocks. In: Lehtinen, M. et al. (eds.), Precambrian Geology of Finland Key to the Evolution of the Fennoscandian Shield. Amsterdam, Elsevier, pp. 343–405. https://doi.org/10.1016/S0166-2635(05)80009-X

Kara, J., Väisänen, M., Johansson, A., Lahaye, Y., O'Brien, H. & Eklund, O., 2018. 1.90-1.88 Ga arc magmatism of central Fennoscandia: geochemistry, U-Pb geochronology, Sm-Nd and Lu-Hf isotope systematics of plutonic-volcanic rocks from southern Finland. Geologica Acta 16, 1−23. https://doi.org/10.1344/GeologicaActa2018.16.1.1

Kara, J., Väisänen, M., Heinonen, J. S., Lahaye, Y., O'Brien, H. & Huhma, H., 2020. Tracing arclogites in the Paleoproterozoic Era – A shift from 1.88 Ga calc-alkaline to 1.86 Ga high-Nb and adakite-like magmatism in central Fennoscandian Shield. Lithos 372, 105663. https://doi.org/10.1016/j.lithos.2020.105663

Keller, C. B., Schoene, B., Barboni, M., Samperton, K. M. & Husson, J. M., 2015. Volcanic–plutonic parity and the differentiation of the continental crust. Nature 523, 301–307. https://doi.org/10.1038/nature14584

Kelley, K. A., Plank, T., Ludden, J. & Staudigel, H., 2003. Composition of altered oceanic crust at ODP Sites 801 and 1149. Geochemistry, Geophysics, Geosystems 4, 1–23. https://doi.org/10.1029/2002GC000435

Kessel, R., Schmidt, M. W., Ulmer, P. & Pettke, T., 2005. Trace element signature of subduction-zone fluids, melts and supercritical liquids at 120–180 km depth. Nature 437, 724–727. https://doi.org/10.1038/nature03971

Konopelko, D., Savatenkov, V., Glebovitsky, V., Kotov, A., Sergeev, S., Matukov, D., Kovach, V. & Zagornaya, N., 2005. Nd isotope variation across the Archaean-Proterozoic boundary in the North Ladoga area, Russian Karelia. GFF 127, 115–122.

Korja, A., Korja, T., Luosto, U. & Heikkinen, P., 1993. Seismic and geoelectric evidence for collisional and extensional events in the Fennoscandian Shield implications for Precambrian crustal evolution. Tectonophysics 219, 129–152. https://doi.org/10.1016/0040-1951(93)90292-R

Korja, A., Lahtinen, R. & Nironen, M., 2006. The Svecofennian orogen: A collage of microcontinents and island arcs. Geological Society, London, Memoirs 32, 561–578. https://doi.org/10.1144/GSL.MEM.2006.032.01.34

Kosunen, P. J., 2004. Petrogenesis of mid-Proterozoic A-type granites: Case studies from Fennoscandia (Finland) and Laurentia (New Mexico). PhD thesis, University of Helsinki, Finland, 21 p. https://helda.helsinki.fi/server/api/core/bitstreams/79cbcd66-9e0f-4e63-8f43-f3843a49d478/content

Kotilainen, A. K., Mänttäri, I., Kurhila, M., Hölttä, P. & Rämö, O. T., 2016. Evolution of a Palaeoproterozoic giant magmatic dome in the Finnish Svecofennian; New insights from U–Pb geochronology. Precambrian Research 272, 39–56. https://doi.org/10.1016/j.precamres.2015.10.023

Kousa, J., Mikkola, P. & Makkonen, H., 2018. Paleoproterozoic mafic and ultramafic volcanic rocks in the South Savo region, eastern Finland. Geological Survey of Finland, Bulletin 407, 63–84. https://doi.org/10.30440/bt407.4

Krystopowicz, N. J. & Currie, C. A., 2013. Crustal eclogitization and lithosphere delamination in orogens. Earth and Planetary Science Letters 361, 195–207. https://doi.org/10.1016/j.epsl.2012.09.056

Kukkonen, I. T. & Lauri, L. S., 2009. Modelling the thermal evolution of a collisional Precambrian orogen: High heat production migmatitic granites of southern Finland. Precambrian Research 168, 233–246. https://doi.org/10.1016/j.precamres.2008.10.004

Kurhila, M., Mänttäri, I., Vaasjoki, M., Rämö, O. T. & Nironen, M., 2011. U–Pb geochronological constraints of the late Svecofennian leucogranites of southern Finland. Precambrian Research 190, 1–24. https://doi.org/10.1016/j.precamres.2011.07.008

Kurhila, M., Vaasjoki, M., Mänttäri, I., Rämö, O. T. & Nironen, M., 2005. U-Pb ages and Nd isotope characteristics of the lateorogenic, migmatizing microcline granites in southwestern Finland. Bulletin of the Geological Society of Finland 77, 105–128. https://www.geologinenseura.fi/sites/geologinenseura.fi/files/kurhilaetal.pdf

Kuusisto, M., Kukkonen, I. T., Heikkinen, P. & Pesonen, L. J., 2006. Lithological interpretation of crustal composition in the Fennoscandian Shield with seismic velocity data. Tectonophysics 420, 283–299. https://doi.org/10.1016/j.tecto.2006.01.014

Lahtinen, R., 2000. Archaean–Proterozoic transition: Geochemistry, provenance and tectonic setting of metasedimentary rocks in central Fennoscandian Shield, Finland. Precambrian Research 104, 147–174. https://doi.org/10.1016/S0301-9268(00)00087-5

Lahtinen, R. & Huhma, H., 1997. Isotopic and geochemical constraints on the evolution of the 1.93-1.79 Ga Svecofennian crust and mantle in Finland. Precambrian Research 82, 13–34. https://doi.org/10.1016/S0301-9268(96)00062-9

Lahtinen, R., Huhma, H. & Kousa, J., 2002. Contrasting source components of the Paleoproterozoic Svecofennian metasediments: Detrital zircon U–Pb, Sm–Nd and geochemical data. Precambrian Research 116, 81–109. https://doi.org/10.1016/S0301-9268(02)00018-9

Lahtinen, R., Huhma, H., Sipilä, P. & Vaarma, M., 2017. Geochemistry, U-Pb geochronology and Sm-Nd data from the Paleoproterozoic Western Finland supersuite – A key component in the coupled Bothnian oroclines. Precambrian Research 299, 264–281. https://doi.org/10.1016/j.precamres.2017.07.025

Lahtinen, R., Korja, A. & Nironen, M., 2005. Paleoproterozoic tectonic evolution. In: Lehtinen, M. et al. (eds.), Precambrian Geology of Finland Key to the Evolution of the Fennoscandian Shield. Amsterdam, Elsevier, pp. 481–531. https://doi.org/10.1016/S0166-2635(05)80012-X

Lahtinen, R., Korja, A., Nironen, M. & Heikkinen, P., 2009. Palaeoproterozoic accretionary processes in Fennoscandia. Geological Society, London, Special Publications 318, 237–256. https://doi.org/10.1144/SP318.8

Lahtinen, R., Salminen, P. E., Sayab, M., Huhma, H., Kurhila, M. & Johnston, S. T., 2022. Age and structural constraints on the tectonic evolution of the Paleoproterozoic Saimaa orocline in Fennoscandia. Precambrian Research 369, 106477. https://doi.org/10.1016/j.precamres.2021.106477

Lahtinen, R., Köykkä, J., Salminen, J., Sayab, M. & Johnston, S. T., 2023. Paleoproterozoic tectonics of Fennoscandia and the birth of Baltica. Earth-Science Reviews 246, 104586. https://doi.org/10.1016/j.earscirev.2023.104586

Lara, P., Oyhantçabal, P. & Dadd, K., 2017. Post-collisional, Late Neoproterozoic, high-Ba-Sr granitic magmatism from the Dom Feliciano Belt and its cratonic foreland, Uruguay: Petrography, geochemistry, geochronology, and tectonic implications. Lithos 277, 178–198. https://doi.org/10.1016/j.lithos.2016.11.026

Lauri, L. S., Andersen, T., Räsänen, J. & Juopperi, H., 2012. Temporal and Hf isotope geochemical evolution of southern Finnish Lapland from 2.77 Ga to 1.76 Ga. Bulletin of the Geological Society of Finland 84, 121–140. https://doi.org/10.17741/bgsf/84.2.002

Lehtonen, M. I., Kujala, H., Kärkkäinen, N., Lehtonen, A., Mäkitie, H., Mänttäri, I., Virransalo, P. & Vuokko, J., 2003. Pre-Quaternary rocks of the South Ostrobothnian Schist Belt. Geological Survey of Finland, Report of Investigation 158, 1–125. https://tupa.gtk.fi/julkaisu/tutkimusraportti/tr_158.pdf

Liégeois, J. P., 1998. Preface—Some words on the post-collisional magmatism. Lithos 45, xv–xvii. https://doi.org/10.1016/S0024-4937(98)00065-6

Liégeois, J. P., Navez, J., Hertogen, J. & Black, R., 1998. Contrasting origin of post-collisional high-K calc-alkaline and shoshonitic versus alkaline and peralkaline granitoids. The use of sliding normalization. Lithos 45, 1–28. https://doi.org/10.1016/S0024-4937(98)00023-1

Lindberg, B. & Eklund, O., 1988. Interactions between basaltic and granitic magmas in a Svecofennian postorogenic granitoid intrusion, Åland, southwest Finland. Lithos 22, 13–23. https://doi.org/10.1016/0024-4937(88)90025-4

Loukola-Ruskeeniemi, K., Hyvönen, E., Airo, M. L., Lerssi, J. & Arkimaa, H., 2023. Country-wide exploration for graphite- and sulphide-rich black shales with airborne geophysics and petrophysical and geochemical studies. Journal of Geochemical Exploration 244, 107123. https://doi.org/10.1016/j.gexplo.2022.107123

Lugmair, G. W. & Carlson, R. W., 1978. The Sm-Nd history of KREEP. Proceedings of the 9th Lunar and Planetary Science Conference. Texas, USA, vol. 2, pp. 689–704.

Mäkitie, H., Sipilä, P., Kujala, H., Lindberg, A. & Kotilainen, A., 2012. Formation mechanism of the Vaasa Batholith in the Fennoscandian shield: Petrographic and geochemical constraints. Bulletin of the Geological Society of Finland 84, 141–166. https://doi.org/10.17741/bgsf/84.2.003

Makkonen, H. V., 2015. Nickel Deposits of the 1.88 Ga Kotalahti and Vammala Belts. In: Maier, W. D. et al. (eds.), Mineral Deposits of Finland. Amsterdam, Elsevier, pp. 253–290. https://doi.org/10.1016/B978-0-12-410438-9.00010-8

Martini, A., Bitencourt, M. F., Weinberg, R. F., De Toni, G. B. & Lauro, V. S. N., 2019. From migmatite to magma—Crustal melting and generation of granite in the Camboriú Complex, south Brazil. Lithos 340, 270–286. https://doi.org/10.1016/j.lithos.2019.05.017

McDonough, W. F. & Sun, S. S., 1995. The composition of the Earth. Chemical geology 120, 223–253. https://doi.org/10.1016/0009-2541(94)00140-4

Meng, F., Gao, S., Song, Z., Niu, Y. & Li, X., 2018. Mesozoic high-Mg andesites from the Daohugou area, Inner Mongolia: Upper-crustal fractional crystallization of parental melt derived from metasomatized lithospheric mantle wedge. Lithos 302, 535–548. https://doi.org/10.1016/j.lithos.2018.01.032

Meissner, R. & Mooney, W., 1998. Weakness of the lower continental crust: a condition for delamination, uplift, and escape. Tectonophysics 296, 47–60. https://doi.org/10.1016/S0040-1951(98)00136-X

Middlemost, E. A. K., 1994. Naming materials in the magma/igneous rock system. Earth-Science Reviews 37, 215–224. https://doi.org/10.1016/0012-8252(94)90029-9

Mikkola, P., Huhma, H., Romu, I. & Kousa, J., 2018. Detrital zircon ages and geochemistry of the metasedimentary rocks along the southeastern boundary of the Central Finland Granitoid Complex. Geological Survey of Finland, Bulletin 407, 28–55. https://doi.org/10.30440/bt407.2

Mohamed, F. H., 1998. Geochemistry and petrogenesis of El Gezira ring complex, Egypt: A monzosyenite cumulate derived from fractional crystallization of trachyandesitic magma. Journal of Volcanology and Geothermal Research 84, 103–123. https://doi.org/10.1016/S0377-0273(98)00034-1

Molnár, F., Middleton, A., Stein, H., O`Brien, H., Lahaye, Y., Huhma, H., Pakkanen, L. & Johanson, B., 2018. Repeated syn- and post-orogenic gold mineralization events between 1.92 and 1.76 Ga along the Kiistala Shear Zone in the Central Lapland Greenstone Belt, northern Finland. Ore Geology Reviews 101, 936–959. https://doi.org/10.1016/j.oregeorev.2018.08.015

Moore, L. J., Murphy, T. J., Barnes, I. L. & Paulsen, P. J., 1982. Absolute Isotopic Abundance Ratios and Atomic Weight of a Reference Sample of Strontium. Journal of Research of the National Bureau of Standards 87, 1–8. https://doi.org/10.6028/jres.087.001

Nandedkar, R. H., Ulmer, P. & Müntener, O., 2014. Fractional crystallization of primitive, hydrous arc magmas: An experimental study at 0.7 GPa. Contributions to Mineralogy and Petrology 167, 1015. https://doi.org/10.1007/s00410-014-1015-5

Nardi, L. V. S., Bitencourt, M. F., Florisbal, L. M. & Padilha, D. F., 2021. Shoshonitic Magmatic Series and the High Ba-Sr Granitoids: A Review with Emphasis on Examples from the Neoproterozoic Dom Feliciano Belt of Southern Brazil and Uruguay. Journal of Earth Science 32, 1359–1373. https://doi.org/10.1007/s12583-021-1534-8

Nevalainen, J., Väisänen, M., Lahaye, Y., Heilimo, E. & Fröjdö, S., 2014. Svecofennian intra-orogenic gabbroic magmatism: A case study from Turku, southwestern

Finland. Bulletin of the Geological Society of Finland 86, 93–112. https://doi.org/10.17741/bgsf/86.2.003

Nikkilä, K., Mänttäri, I., Nironen, M., Eklund, O. & Korja, A., 2016. Three stages to form a large batholith after terrane accretion – An example from the Svecofennian orogen. Precambrian Research 281, 618–638. https://doi.org/10.1016/j.precamres.2016.06.018

Nironen, M., 1997. The Svecofennian Orogen: A tectonic model. Precambrian Research 86, 21–44. https://doi.org/10.1016/S0301-9268(97)00039-9

Nironen, M., 2005. Proterozoic orogenic granitoid rocks. In: Lehtinen, M. et al. (eds.), Precambrian Geology of Finland Key to the Evolution of the Fennoscandian Shield. Amsterdam, Elsevier, pp. 443–479. https://doi.org/10.1016/S0166-2635(05)80011-8

Nironen, M., 2017. Guide to the Geological Map of Finland – Bedrock 1:1 000 000. Geological Survey of Finland, Special Paper 60, 41–76. https://tupa.gtk.fi/julkaisu/specialpaper/sp_060_pages_041_076.pdf

Nironen, M., Elliott, B. A. & Rämö, O. T., 2000. 1.88–1.87 Ga post-kinematic intrusions of the Central Finland Granitoid Complex: A shift from C-type to A-type magmatism during lithospheric convergence. Lithos 53, 37–58. https://doi.org/10.1016/S0024-4937(00)00007-4

Pajunen, M., 2008. Tectonic evolution of the Svecofennian crust in southern Finland: A basis for characterizing bedrock technical properties. Geological Survey of Finland, Special Paper 47, 1–326. https://tupa.gtk.fi/julkaisu/specialpaper/sp_047.pdf

Palin, R. M., White, R. W., Green, E. C. R., Diener, J. F. A., Powell, R. & Holland, T. J. B., 2016. High-grade metamorphism and partial melting of basic and intermediate rocks. Journal of Metamorphic Geology 34, 871–892. https://doi.org/10.1111/jmg.12212

Papunen, H., 1986. Suomen metalliset malmiesiintymät. In: Papunen, H. et al. (eds.), Suomen malmigeologia: metalliset malmiesiintymät. Geological Society of Finland, Espoo, pp. 133–214 (in Finnish).

Patchett, J. & Kouvo, O., 1986. Origin of continental crust of 1.9-1.7 Ga age: Nd isotopes and U-Pb zircon ages in the Svecokarelian terrain of South Finland. Contributions to Mineralogy and Petrology 92, 1–12. https://doi.org/10.1007/BF00373959

Peccerillo, A. & Taylor, S. R., 1976. Geochemistry of eocene calc-alkaline volcanic rocks from the Kastamonu area, Northern Turkey. Contributions to Mineralogy and Petrology 58, 63–81. https://doi.org/10.1007/BF00384745

Pekkarinen, L., 2002. Haukivuori and Pieksämäki. Explanation to the Geological map of Finland 1: 100 000, pre-Quaternary rocks, sheet 3231 and 3231, 98 p (in Finnish with English summary). https://tupa.gtk.fi/kartta/kallioperakartta100/kps_3231_3232.pdf

Peltonen, P., O'Brien, H., Karhu, J. & Kukkonen, I., 2000. Kimberlites, carbonatites, and their mantle sample: Constraints for the origin and temporal evolution of the lithospheric mantle in Fennoscandia. In: Pesonen, L. J. et al. (eds.), Proceedings of the 1th Symposium on the Structure, Composition and Evolution of the Lithosphere in Finland. Espoo, Finland, pp. 63–69. https://www.seismo.helsinki.fi/pdf/Lito2000.pdf

Peltonen, P., 2005. Svecofennian mafic-ultramafic intrusions. In: Lehtinen, M. et al. (eds.), Precambrian Geology of Finland Key to the Evolution of the Fennoscandian Shield. Amsterdam, Elsevier, pp. 407–441. https://doi.org/10.1016/S0166-2635(05)80010-6

Peltonen, P. & Mänttäri, I., 2001. An ion microprobe U-Th-Pb study of zircon xenocrysts from the Lahtojoki kimberlite pipe, eastern Finland. Bulletin of the Geological Society of Finland 73, 47–58. https://doi.org/10.17741/bgsf/73.1-2.004

Pesonen, L. J., Elming, S. Å., Mertanen, S., Pisarevsky, S., D'Agrella-Filho, M. S., Meert, J. G., Schmidt, P. W., Abrahamsen, N. & Bylund, G., 2003. Palaeomagnetic configuration of continents during the Proterozoic. Tectonophysics 375, 289–324. https://doi.org/10.1016/S0040-1951(03)00343-3

Plank, T., 2014. The Chemical Composition of Subducting Sediments. In: Holland, H. D. & Turekian, K. K. (eds.), Treatise on Geochemistry (Second Edition). Amsterdam, Elsevier, pp. 607–629. https://doi.org/10.1016/B978-0-08-095975-7.00319-3

Qian, Q., Chung, S. L., Lee, T. Y. & Wen, D. J., 2003. Mesozoic high-Ba–Sr granitoids from North China: Geochemical characteristics and geological implications. Terra Nova 15, 272–278. https://doi.org/10.1046/j.1365-3121.2003.00491.x

Rämö, O. T. & Haapala, I., 2005. Rapakivi Granites. In: Lehtinen, M. et al. (eds.), Precambrian Geology of Finland Key to the Evolution of the Fennoscandian Shield. Amsterdam, Elsevier, pp. 533–562. https://doi.org/10.1016/S0166-2635(05)80013-1

Rasilainen, K., Eilu, P., Ahtola, T., Halkoaho, T., Kärkkäinen, N., Kuusela, J., Lintinen, P. & Törmänen, T., 2018. Quantitative assessment of undiscovered resources in lithium–caesium–tantalum pegmatite-hosted deposits in Finland. Geological Survey of Finland, Bulletin 406, 31 p. https://doi.org/10.30440/bt406

Rasilainen, K., Eilu, P., Ahtola, T., Feltrin, L., Halkoaho, T., Kuusela, J., Lintinen, P., Niiranen, T. & Törmänen, T., 2023. Quantitative assessment of undiscovered resources in carbonatite and peralkaline intrusion-related REE–P deposits in Finland. Geological Survey of Finland, Bulletin 415, 37 p. https://doi.org/10.30440/bt415

Richard, P., Shimizu, N. & Allègre, C. J., 1976. 143Nd/146Nd, a natural tracer: An application to oceanic basalts. Earth and Planetary Science Letters 31, 269–278. https://doi.org/10.1016/0012-821X(76)90219-3

Rocchi, S., Di Vincenzo, G., Ghezzo, C. & Nardini, I., 2009. Granite-lamprophyre connection in the latest stages of the early Paleozoic Ross Orogeny (Victoria Land, Antarctica). GSA Bulletin 121, 801–819. https://doi.org/10.1130/B26342.1

Rubatto, D., 2002. Zircon trace element geochemistry: Partitioning with Garnet and the link between U–Pb ages and metamorphism. Chemical Geology 184, 123–138. https://doi.org/10.1016/S0009-2541(01)00355-2

Rukhlov, A. S. & Bell, K., 2010. Geochronology of carbonatites from the Canadian and Baltic Shields, and the Canadian Cordillera: Clues to mantle evolution. Mineralogy and Petrology 98, 11–54. https://doi.org/10.1007/s00710-009-0054-5

Rutanen, H. & Andersson, U. B., 2009. Mafic plutonic rocks in a continental-arc setting: geochemistry of 1.87–1.78 Ga rocks from south-central Sweden and models of their palaeotectonic setting. Geological Journal 44, 241–279. ru

Rutanen, H., Andersson, U. B., Väisänen, M., Johansson, Å., Sören, F. & Lahaye, Y., 2011. 1.8 Ga magmatism in southern Finland: Strongly enriched mantle and juvenile crustal sources in a post-collisional setting. International Geology Review 53, 1622–1683. https://doi.org/10.1080/00206814.2010.496241

Saalmann, K., Mänttäri, I., Ruffet, G. & Whitehouse, M. J., 2009. Age and tectonic framework of structurally controlled Palaeoproterozoic gold mineralization in the Häme belt of southern Finland. Precambrian Research 174, 53–77. https://doi.org/10.1016/j.precamres.2009.06.005

Sekine, T. & Wyllie, P. J., 1982. Phase relationships in the system KAlSiO4-Mg2SiO4-SiO2-H2O as a model for hybridization between hydrous siliceous melts and peridotite. Contributions to Mineralogy and Petrology 79, 368–374. https://doi.org/10.1007/BF01132066

Simonen, A., 1980. The Precambrian Finland. Geological Survey of Finland, Bulletin 304, 58 p. https://tupa.gtk.fi/julkaisu/bulletin/bt_304.pdf

Sipilä, P., Björk, L., Kero, L., Kujala, H., Lindberg, A. & Virransalo, P., 2017. Bedrock geology of the Kvarken area. Geological Survey of Finland, Public archive report 61, 1–38. https://tupa.gtk.fi/raportti/arkisto/61_2017.pdf

Sisson, T. W., Ratajeski, K., Hankins, W. B. & Glazner, A. F., 2005. Voluminous granitic magmas from common basaltic sources. Contributions to Mineralogy and Petrology 148, 635–661. https://doi.org/10.1007/s00410-004-0632-9

Spandler, C. & Pirard, C., 2013. Element recycling from subducting slabs to arc crust: A review. Lithos 170, 208–223. https://doi.org/10.1016/j.lithos.2013.02.016

Spandler, C., Mavrogenes, J. & Hermann, J., 2007. Experimental constraints on element mobility from subducted sediments using high-P synthetic fluid/melt inclusions. Chemical Geology 239, 228–249. https://doi.org/10.1016/j.chemgeo.2006.10.005

Steiger, R. H. & Jäger, E., 1977. Subcommission on geochronology: Convention on the use of decay constants in geo- and cosmochronology. Earth and Planetary Science Letters 36, 359–362. https://doi.org/10.1016/0012-821X(77)90060-7

Suikkanen, E., Huhma, H., Kurhila, M. & Lahaye, Y., 2014. The age and origin of the Vaasa migmatite complex revisited. Bulletin of the Geological Society of Finland 86, 41–55. https://doi.org/10.17741/bgsf/86.1.003

Sundblad, K., Salin, E., Claesson, S., Gyllencreutz, R. & Billström, K., 2021. The Precambrian of Gotland, a key for understanding the Proterozoic evolution in southern Fennoscandia. Precambrian Research 363, 106321. https://doi.org/10.1016/j.precamres.2021.106321

Tarney, J. & Jones, C. E., 1994. Trace element geochemistry of orogenic igneous rocks and crustal growth models. Journal of the Geological Society 151, 855–868. https://doi.org/10.1144/gsjgs.151.5.0855

Taylor, S. R. & McLennan, S. M., 1995. The geochemical evolution of the continental crust. Reviews of Geophysics 33, 241–265. https://doi.org/10.1029/95RG00262

Thompson, R. N. & Fowler, M. B., 1986. Subduction-related shoshonitic and ultrapotassic magmatism: A study of Siluro-Ordovician syenites from the Scottish Caledonides. Contributions to Mineralogy and Petrology 94, 507–522. https://doi.org/10.1007/BF00376342

Torppa, A. & Karhu, J. A., 2013. Stable isotope and trace element constraints to the origin of carbonate rocks in the Korsnäs Pb-REE deposit, western Finland. In: Johnsson, E. (ed.), Proceedings of the 12th Biennial SGA Meeting, Uppsala, Sweden, vol. 4, pp. 1746–1749.

Turner, S. J. & Langmuir, C. H., 2022. Sediment and ocean crust both melt at subduction zones. Earth and Planetary Science Letters 584, 117424. https://doi.org/10.1016/j.epsl.2022.117424

Vaasjoki, M., Huhma, H., Lahtinen, R. & Vestin, J., 2003. Sources of Svecofennian granitoids in the light of ion probe U-Pb measurements on their zircons. Precambrian Research 121, 251–262. https://doi.org/10.1016/S0301-9268(03)00015-9

Vermeesch, P., 2018. IsoplotR: A free and open toolbox for geochronology. Geoscience Frontiers 9, 1479–1493. https://doi.org/10.1016/j.gsf.2018.04.001

Villa, I. M., De Bièvre, P., Holden, N. E. & Renne, P. R., 2015. IUPAC-IUGS recommendation on the halflife of 87Rb. Geochimica et Cosmochimica Acta 164, 382–385. https://doi.org/10.1016/j.gca.2015.05.025

Väisänen, M. & Mänttäri, I., 2002. 1.90-1.88 Ga arc and back-arc basin in the Orijärvi area, SW Finland. Bulletin of the Geological Society of Finland 74, 185–214. https://doi.org/10.17741/bgsf/74.1-2.009

Väisänen, M., Mänttäri, I., Kriegsman, L. M. & Hölttä, P., 2000. Tectonic setting of post-collisional magmatism in the Palaeoproterozoic Svecofennian Orogen, SW Finland. Lithos 54, 63–81. https://doi.org/10.1016/S0024-4937(00)00018-9

Väisänen, M., Eklund, O., Lahaye, Y., O'Brien, H., Fröjdö, S., Högdahl, K. & Lammi, M., 2012. Intra-orogenic Svecofennian magmatism in SW Finland constrained by

LA-MC-ICP-MS zircon dating and geochemistry. GFF 134, 99–114. https://doi.org/10.1080/11035897.2012.680606

Wahlgren, C. H. & Stephens, M. B., 2020. Småland lithotectonic unit dominated by Paleoproterozoic (1.8 Ga) syn-orogenic magmatism, Svecokarelian orogen. Geological Society, London, Memoirs 50, 207–235. https://doi.org/10.1144/M50-2017-19

Whalen, J. B., Currie, K. L. & Chappell, B. W., 1987. A-type granites: Geochemical characteristics, discrimination and petrogenesis. Contributions to Mineralogy and Petrology 95, 407–419. https://doi.org/10.1007/BF00402202

Woodard, J. & Hölttä, P., 2005. The Naantali alvikite vein-dykes: A new carbonatite in southwestern Finland. Geological Survey of Finland, Special Paper 38, 5–10. https://tupa.gtk.fi/julkaisu/specialpaper/sp_038.pdf

Woodard, J. & Huhma, H., 2015. Paleoproterozoic mantle enrichment beneath the Fennoscandian Shield: Isotopic insight from carbonatites and lamprophyres. Lithos 236, 311–323. https://doi.org/10.1016/j.lithos.2015.09.009

Woodard, J., Kietäväinen, R. & Eklund, O., 2014. Svecofennian post-collisional shoshonitic lamprophyres at the margin of the Karelia Craton: Implications for mantle metasomatism. Lithos 205, 379–393. https://doi.org/10.1016/j.lithos.2014.06.021

Wyllie, P. J. & Sekine, T., 1982. The formation of mantle phlogopite in subduction zone hybridization. Contributions to Mineralogy and Petrology 79, 375–380. https://doi.org/10.1007/BF01132067

Ye, H. M., Li, X. H., Li, Z. X. & Zhang, C. L., 2008. Age and origin of high Ba–Sr appinite–granites at the northwestern margin of the Tibet Plateau: Implications for early Paleozoic tectonic evolution of the Western Kunlun orogenic belt. Gondwana Research 13, 126–138. https://doi.org/10.1016/j.gr.2007.08.005

Yliniemi, J., Kozlovskaya, E., Hjelt, S. E., Komminaho, K. & Ushakov, A., 2004. Structure of the crust and uppermost mantle beneath southern Finland revealed by analysis of local events registered by the SVEKALAPKO seismic array. Tectonophysics 394, 41–67. https://doi.org/10.1016/j.tecto.2004.07.056

Zhang, Y., Sun, M., Yuan, C., Xu, Y., Long, X., Tomurhuu, D., Wang, C. Y. & He, B., 2015. Magma mixing origin for high Ba–Sr granitic pluton in the Bayankhongor area, central Mongolia: Response to slab roll-back. Journal of Asian Earth Sciences 113, 353–368. https://doi.org/10.1016/j.jseaes.2014.11.029